UNIVERSITY OF MOLISE

Dept. of Medicine and Health Science "V. Tiberio"

PhD course in TRANSLATIONAL AND CLINICAL MEDICINE
XXX CYCLE

S.S.D: Area-05-Bio 14 Farmacologia

Doctoral Thesis

GENETIC, PATHOPHYSIOLOGICAL, AND PHARMACOLOGICAL IMPLICATIONS OF KCNT1 AND KCNT2 POTASSIUM CHANNELS IN NEURODEVELOPMENTAL DISORDERS AND EPILEPTIC ENCEPHALOPATHIES

Tutor:
Prof. Maurizio Taglialatela

Student:
Laura Manocchio

Coordinator:
Prof. Ciro COSTAGLIOLA

Academic year: 2016/2017

INDEX

ABBREVIATIONS

EE: Epileptic Encephalopathy

NEE: Neonatal Epileptic Encephalopathy

MMPSI: Malignant Migrating Partial Seizure of Infancy

ADNFLE: Autosomal Dominant Nocturnal Frontal Lobe Epilepsy

RCK: Regulators of K^+ Conductance

CHO: Chinese Hamster Ovary

HEK: Human Embryonic Kidney

RT: Room Temperature

GOF: Gain-of-function

INTRODUCTION

1. The Potassium channels family

Potassium channels (K^+) are membrane proteins that allow rapid and selective flow of K^+ ions across the cell membrane, thus generating electrical signals in many excitable or unexcitable cells. Potassium channels play an important role in several biological functions: their contribution is important in determining the shape and the duration of the action potential, in the control of the membrane potential, in the modulation of hormone secretion and epithelial function.

The potassium channel family can be classified based on their structure in channels with two transmembrane segments (2TM), four transmembrane segments (4TM; 2-pore domain), six transmembrane segments (6TM; voltage-gated K^+ channels and SK) or seven transmembrane segments (7TM; SLO, Figure 1).

The inward rectifier (K_{ir}) family contains subunits with a topological structure characterized by two TM segments flanking the pore-forming domain; they assemble as tetramers. They are involved in the control of several biological functions in different cell types, such as cardiac myocytes and endothelial cells.

The two-pore 4TM segments K^+ channels (K_{2P}) family assemble as dimers and play an important role in several neuronal functions.

The 6TM segments (called from S_1 to S_6) K^+ channels family includes several subfamilies called from Kv1.x to Kv12.x. Voltage-dependent K^+ channels contain a voltage-sensor domain (VSD; from S_1 to S_4 segments) with the S_4 segment containing positively-charged amino acids that constitute the voltage-sensing elements. The small conductance K^+ channel family (SK channels, SKCa, KCa2) also have 6TM and are activated by an increase in intracellular Ca^{2+} ions [Gonzalez et al., 2012].

In particular, the SLO channel subfamily will be the focus of the present Doctoral Thesis and will be extensively discussed in the next sessions.

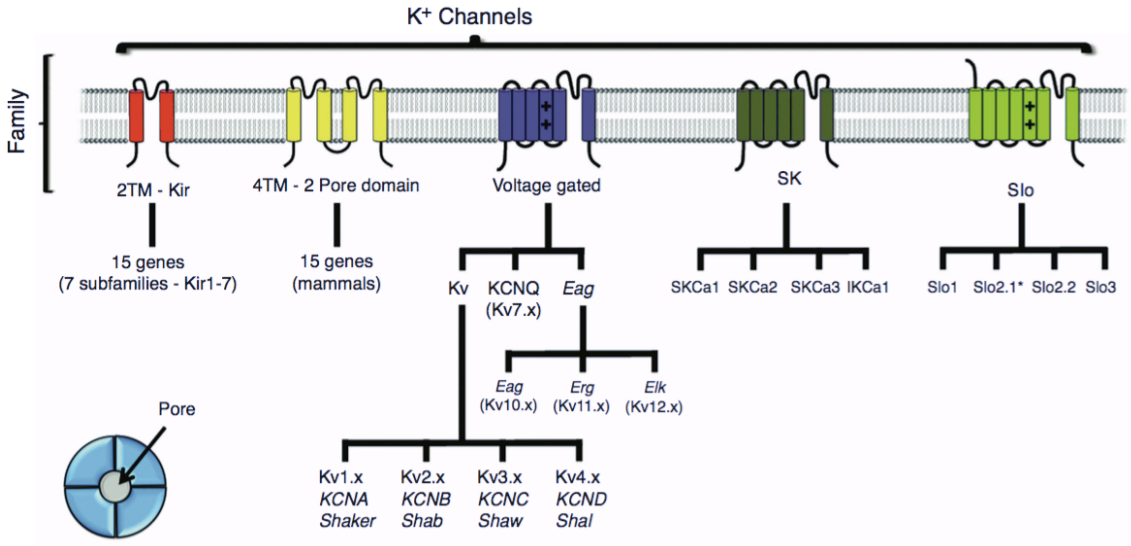

Figure 1 Potassium channels family classification accordingly to their subunit structure. Potassium channel families are classified in those having two transmembrane domains (2TM; K_{ir}), 4TM (2-pore domain), 6TM (voltage-gated and SK) and 7TM (SLO). The large-conductance SLO channel family include the SLO2.x channels, which have a topological structure showing six transmembrane domains. [From *Gonzalez et al., 2012*].

1.1 The SLO (K_{Ca}) family of K^+ channels

The SLO family encompasses four genes in the mammalian genome that code for high-conductance K^+ channels (Table 1). The first member of this family, SLO1, is also known as "big" K^+ channel (BK) or maxi-K channels as these channels have an unusual large conductance (about 250 pS). Other two highly similar SLO2 paralogues, SLO2.1 (also known as Slick, KCNT2 or calcium-activated K^+ channels 4.2) and SLO2.2 (also known as Slack, KCNT1 or calcium-activated K^+ channels 4.1) are members of the SLO2 channels family. The last member of SLO family is called SLO3. All four genes encode α-subunits that forms heterotetrameric channels that gate a K^+-selective current, with marked differences in their gating properties [Salkoff et al., 2006], as detailed below:

Channel	Alternative names	Gene symbol (human)	Chromosomal localization
SLO1	BK, K_{Ca}, Maxi-K, KCa1.1	KCNMA1	10q22
SLO2.1	Slick, K_{Na}, KCa4.2	KCNT2	1q31.3
SLO2.2	Slack, K_{Na}, KCa4.1	KCNT1	9q34.3
SLO3	Potassium large conductance pH-sensitive channel, KCa5.1	KCNU1	8p11.2

Table 1 SLO channels family genes. [Adapted from *Salkoff et al., 2006*].

SLO1: SLO1 channels are expressed in many tissues where they elicited an outward K^+ current with an unusual dependence on both membrane depolarization and influx of Ca^{2+} ions [Gorman et al.,1980]. The SLO1 gene was cloned from the *Drosophila* mutants *Slowpoke*, which exhibited flight problems and altered response to heat shock. Voltage-clamp recordings of currents recorded in *Drosophila* mutant revealed that the calcium-dependent regulation of the outward K^+ current was absent. The SLO1 gene codes for a protein with homology to voltage-dependent K^+ channels, but it has an extra TM segment (S_0), allowing the N-terminus to face the extracellular side of the membrane. In addition, these channels also contain hydrophobic domains at the C-terminus, called RCK (Regulators of K^+ conductance): when Ca^{2+} ions bind these sites, the membrane depolarization needed to open channel decreases, rending SLO1 both Ca^{2+}- and voltage-

dependent channels.

SLO2 is the second member of the SLO channels family that include two paralogues called KCNT1 and KCNT2. Functional studies have revealed that KCNT1 and KCNT2, similarly to BK channels, have high conductance but, differently from BK are potentiated by Na^+ (not Ca^{2+}) ions, thereby underlying Na^+-activated K^+ currents (IK_{Na}). These currents have been described in many cells [Hartung et al., 1985], including guinea pig cardiomyocytes [Kameyama et al., 1984] and a wide variety of mammalian neurons, such as those located in the dorsal root ganglia (DRG) [Bischoff et al., 1998].

The identification of the Na^+-activated K^+ currents has been achieved by means of different experimental tools; including the replacement of the external sodium by lithium ions. Lithium is a much weaker activator of K_{Na} channels than sodium. Because lithium promptly enters cells through voltage-dependent sodium channels, lithium replacement in voltage-clamp experiments reduces the net outward currents if K_{Na} currents are present [Hage et al., 2012].

The IK_{Na} currents are believed to play an important role under ischemic conditions in cardiomyocytes, due to a protective role prompted by the activation of large K^+ conductances upon dangerous increase in $[Na^+]_i$ [Mitani et al., 1992]. Similarly, in many neurons I_{KNa} currents contribute to a long-lasting slow afterhyperpolarization (sAHP), which results from a slowly developing outward current evoked during sustained stimulation. The period of reduced excitability afforded by sAHP is thought to protect the cell from repetitive and tetanic activity. It has been shown that, whereas the early part of sAHP is dependent on Ca^{2+} influx during stimulation, the late part of sHAP is Na^+ sensitive [Schwindt et al., 1998a,b]. Similar Na^+-dependent sHAP has also been observed in a number of other neurons, such as hippocampal pyramidal cells [Gustafsson and Wigstrom, 1983] and spinal cord neurons [Wallen et al., 2007].

The fact that KCNT1 and KCNT2 represent the molecular basis of IK_{Na} currents has been confirmed in mouse models lacking both SLO2.2 and SLO2.1 genes: these mice show a complete absence of the K_{Na} current in DRG neurons, which promotes an increased excitability in response to depolarizing stimuli. This increased neuronal firing is thought to be responsible for the enhanced itching and pain sensations observed in this mouse

model [Martinez-Espinosa et al., 2015].

SLO3 is the third member of the SLO family channel. The SLO3 gene was identified by bioinformatic approaches characterizing an EST (expressed sequence tag) encoding a sequence with high similarity to the SLO1 channels. Like SLO2, SLO3 channels lack the Ca^{2+}-dependent gating but they are dependent on internal pH values (Figure 2).

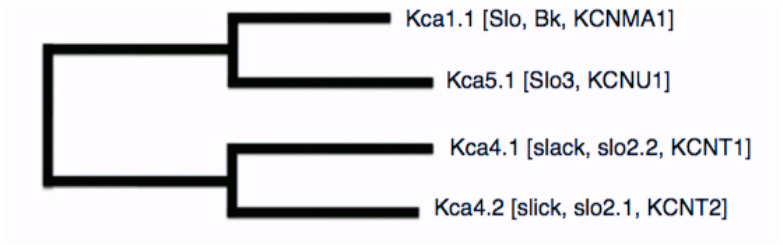

Figure 2 Phylogenetic tree of SLO channels family in mammals. *[From: Gonzalez et al., 2012].*

1.2 Topological structure of the SLO2 α-subunits

The topological structure of the α-subunits of SLO2 channels resembles that of voltage-gated K^+ channels in having a symmetrical arrangement of membrane-spanning segments clustered around a water-filled, K^+ ion-selective pore.

The α-subunit of SLO2 channels has six hydrophobic transmembrane segments (S_1-S_6) along with a pore-lining loop that is found between the S_5-S_6 segments. The SLO2 channels also exhibit a large C-terminal region (over 900 amino acids in length) that greatly exceeds the length of the region encompassing the membrane-spanning domains and contains both hydrophobic and hydrophilic domains. Both SLO2.1 and SLO2.2 channels lack the canonical gating charges in the S_4 membrane-spanning segment usually associated with voltage sensing and both exhibit a low intrinsic voltage dependence of activation [Yuan et al., 2003]. The N- and C-terminus of SLO2 channels are located on the intracellular side. The C-terminus of SLO2 subunits contains two predicted regulators of K^+ conductance (RCK) domains that stack on the top of each other and form a gating ring underneath the channel pore (Figure 3). X-ray crystallographic studies of C-terminal domain of chicken KCNT1 channels have confirmed that the structure of RCK domains is likely to resemble that of SLO1 channels.

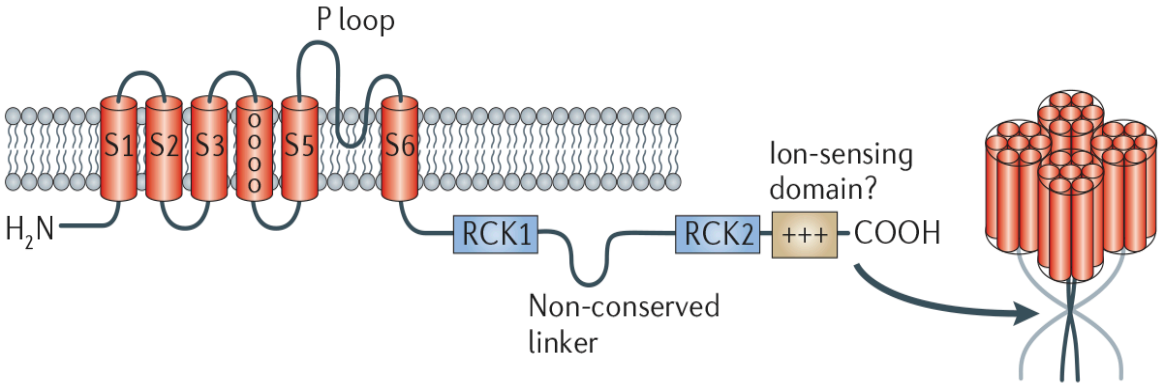

Figure 3 Topological structure of SLO2 α-subunit. SLO2 channels have six transmembrane domains. The transmembrane domains are labeled as S_1-S_6, with the P-loop located between the S_5-S_6 segments. Both the N- and C-terminal ends are cytosolic. The C-terminal domain contains two Regulators of K^+ conductance (RCK). The S_4 segment lack the canonical positive charges that confers voltage sensitivity. Four of these α subunits assemble into a functional channel. (Adapted from: *Salkoff et al., 2006*).

More recently, structural studies have revealed with high accuracy the transition of the KCNT1 channels into the open configuration as a function of Na^+ concentration: in fact, by using Cryo-Electron Microscopy, MacKinnon and coll. (2017) solved the crystal structure of KCNT1 channels in the open configuration and revealed structural features that were not present in the closed configuration of KCNT1 channels. In particular, in the open configuration, the gating ring is firmly compressed against the transmembrane domain. In addition, a subdomain structure of the membrane-facing surface of the gating ring (RCK1 N-lobe) showed an expanded conformation induced by Na^+ ions, if compared to the closed configuration. This structure is also responsible for pore opening, by causing the displacement of the S_6 helices radially away from the pore axis [Hite et al., 2017]. By contrast, in the closed and Na^+-unbound state, the S_6 helices were found to be constricted, thus leading to the observation that the channel was closed (Figure 4). Such observation was also supported by the absence of channels activity in membrane with 0 mM cytoplasmic Na^+ [Hite et al., 2015].

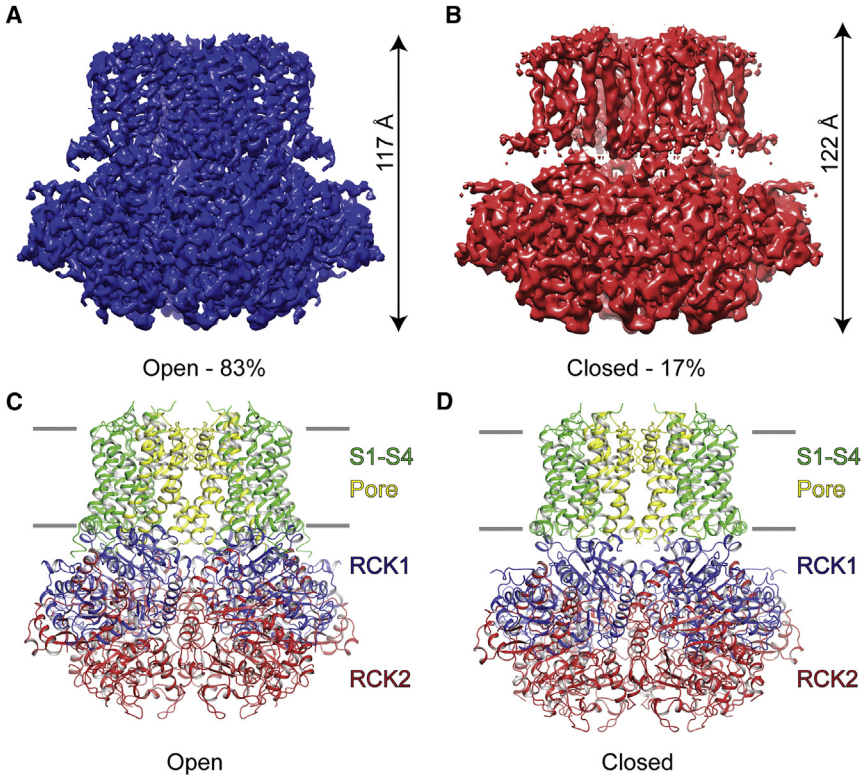

Figure 4 Architecture of closed and open KCNT1 channel subunits by cryo-electron microscopy. (A, B) Cryo EM density map of open (A) and closed (B) KCNT1 channel. (C, D**)** Domain organization of open (A) and closed (B) chicken KCNT1. The S_1-S_4 domains are colored in green, the pore domain is yellow, the RCK 1 domain is blue and the RCK2 domain is red. [From: *Hite et al., 2017*]

1.3 SLO2.2 (or KCNT1 or Slack) channels

The term "Slack" derived from "sequence like A calcium activated K^+ channels" because part of the pore domain and the S_6 domain is similar to that of SLO1 (BK) large conductance calcium-activated K^+ channels [Dryer, 1994].

KCNT1 channel was first cloned and expressed in 1998 [Joiner et al., 1998] and was found to be regulated by intracellular Na^+ ions in 2003 [Yuan et al., 2003]. KCNT1 channels elicit outwardly rectifying K^+ currents that increase upon depolarization. These currents show complex activation kinetics, with an instantaneous time-independent component, followed by a slower, time-dependent one.

When expressed either in mammalian cell lines or *Xenopus* oocytes KCNT1 channels have a relatively large unitary conductance (~180 pS) [Yuan et al., 2003]; in addition, multiple subconductance states have been described [Brown et al., 2008].

In these experimental conditions, the half-maximal concentration for $[Na^+]_i$-dependent

activation of KCNT1 channels is ~ 40 mM [Tamsett et al., 2009], a concentration highly overpassing physiological Na^+ levels but possibly occurring during high frequency neuronal activity or upon hypoxic insults. These observations suggest that the role of K_{Na} channels may be strictly limited to these physiopathological conditions. However, it has to be highlighted that another activator of KCNT1 current is the nicotinamide adenine dinucleotide (NAD^+) [Tamsett et al., 2009], which induces a significant reduction in the $[Na^+]_i$ required for current activation and likely allows KCNT1 current activation also in physiological conditions. These observations are supported by the fact that both Na^+ and NAD^+ binding sites are localized in the RCK2 domain. In particular, the D818 and H823 residues of rat KCNT1 channels are crucial for the Na^+ sensitivity of KCNT1 currents [Zhang et al., 2010], while a complex domain appears to be crucial for NAD^+ binding.

KCNT1 channel subunits also contain a PDZ-binding consensus motif at the end of the C-terminus, which is functionally relevant since Na^+ channels and glutamate receptors can cluster by binding to the same domain [Tomita et al., 2001].

Different KCNT1 channel subunits are generated by alternative splicing of KCNT1 mRNA. In fact, five different transcripts from the rat KCNT1 gene have been described, and these are predicted to produce KCNT1 channels that differ in their cytoplasmic amino termini. In particular, the N-terminal domain of Slack-A is smaller than that of Slack-B and the sequence of Slack-A N-terminal domain very closely resembles the N-terminus of the KCNT2 subunits.

In functional experiments, these isoforms show different activation kinetics: in fact, while Slack-B subunits elicited very slowly-activating currents, Slack-A channels activate very rapidly upon depolarization [Joiner et al., 1998; Yuan et al., 2003].

The kinetic properties of Slack-A and Slack-B isoforms indicate that the predominance of one or the other of these two isoforms is likely to shape the specific pattern of response to repetitive stimulation, as observed in simulations performed in neuronal models: in particular, Slack-B channels are likely to promote bursting and a graded pattern of adaptation, whereas Slack-A channels produce a strong and fixed pattern of rapid adaptation [Brown et al., 2008].

1.4 SLO2.1 (or KCNT2 or Slick) channels

The term "Slick" stands for "sequence like an intermediate conductance K^+ channel" as KCNT2 channels have a conductance that is intermediate between that of SLO1 (BK) calcium-activated K^+ channels and other K^+ channels.

Overall, the sequence of KCNT2 channel is 74% identical to that of KCNT1; the transmembrane domains and the RCK domains are almost identical. The greatest divergence between KCNT1 and KCNT2 channels occurs at the distal C-terminal regions. The predicted cytoplasmic N-terminus of KCNT2 is similar to that of the Slack-A isoform.

Also the electrophysiological properties of KCNT2 currents, recorded in mammalian cells or *Xenopus* oocytes, resemble those of Slack-A: in fact, KCNT2 channels activate very rapidly upon depolarization and have multiple subconductance states. Also, KCNT2 currents are activated by Na^+ ions in a concentration-dependent and reversible manner. Concentration-response curves for activation of KCNT2 channels revealed that the effective Na^+ concentrations for 50% (EC_{50}) of KCNT2 channels activation is 89 mM, a value even greater than that described for KCNT1 channels activation (40 mM). By contrast, whereas KCNT1 channels activation has an absolute requirement of Na^+ ions, KCNT2 channels have a basal level of activity even in the absence of Na^+ ions [Bhattacharjee et al., 2003].

In addition to their Na^+-sensitivity, both KCNT1 and KCNT2 channel subunits can be activated by intracellular chloride ions (Cl^-) [Yuan et al., 2000], although there is a large difference in their sensitivity: in fact, there is an approximately five-fold increase in KCNT2 channel activation when cytoplasmic Cl^- is raised from 3 to 130 mM in the presence of 5 mM Na^+, whereas KCNT1 channel activity is increased only twofold under the same conditions [Bhattacharjee et al., 2003].

The domains that confer the Cl^- sensitivity are yet unknown. It has been proposed that, in SLO2, Cl^- binds to a stretch of positively charged amino acids that has been referred as "Cl^- bowl", localized in the tail region of the channel [Yuan et al., 2000].

The KCNT2 channels are considered to be hybrid between two classes of K^+ channels: Na^+-activated (K_{Na}) and ATP-sensitive (K_{ATP}) K^+ channels. Indeed, KCNT2 channel subunits also contain a regulatory nucleotide-binding site that is responsible for ATP-mediated inhibition of channel activity, thus suggesting a more specialized protective

role under ischemic conditions and seizure activity in neuronal cells. The ATP-binding site is located in the second RCK domain, making the channel sensitive to cytoplasmic ATP levels [Bhattacharjee et al., 2003]. Like KCNT1, also currents elicited by KCNT2 subunits are potentiated by NAD^+ exposure. The NAD binding motif in these channels seem to be located within the second RCK domain of KCNT1 and KCNT2 subunits and includes a "finger-print region" containing $\beta\alpha\beta\alpha\beta$ motif [Tamsett et al.,2009].

1.5 KCNT1 and KCNT2 channel subunits forms heteromeric complexes

Slack and Slick subunits can coassemble to form heterotetrameric channels that differ in their properties from those of homomeric channels [Chen et al., 2009]. The unitary conductance of Slack/Slick heteromeric channels results to be intermediate between that of Slack (~ 180 pS) and Slick (~ 140 pS) homomers. Moreover, assembly of heteromeric Slack/Slick channels appears to be specific for the Slack-B isoform: in fact, when Slick and Slack-B are coexpressed at 1:1 ratio, either in *Xenopus* oocytes or in mammalian HEK293 cells, a 18-25 fold increase in current amplitude is observed when compared to the currents expressed by either subunit alone [Chen et al., 2009]. This functional effect is due to an increased protein expression at the plasma membrane (as demonstrated in biotinylation experiments). These results were obtained by using chimeric channels that replaced the cytoplasmatic N-terminal domain of KCNT2 with that of Slack-B. The coexpression of this modified Slick channel with wild-type Slick channels in oocytes produced a 30-fold increase in whole-oocyte currents, which is similar to the increase obtained when Slack-B subunits were co-expressed with Slick.
Interaction between Slack-B and Slick subunits was also demonstrated by co-immunoprecipitation experiments in rat brain tissue and in heterologous expression system [Chen et al., 2009].

1.6 KCNT1 and KCNT2 channels regulation

The activity of KCNT1 and KCNT2 channel subunits, as well as the heterotetrameric KCNT1/KCNT2 channel assembly, is regulated by several signaling pathways:

- Modulation of KCNT1 and KCNT2 by Protein Kinase C (PKC)

Exposure of mammalian cells or *Xenopus* oocytes expressing KCNT1 channels to activators of protein kinase C (PKC) such as diacylglycerol or phorbol esters, lead to a 2-3 fold increase in current amplitude and a slowing of the rate of activation [Santi et al., 2006]. The PKC-mediated effects involved the phosphorylation of many residues, such as serine residue S407 located in the region of the cytoplasmic C-terminal domain between the S_6 transmembrane segment and the first RCK domain [Barcia et al., 2012] and the T517 residue located in the RCK domain [Santi et al., 2006].

In contrast to KCNT1 channels, the PKC activation induces a decrease in KCNT2 currents and this effect seems to be mediated by modification within the C-terminus of the channels [Santi et al., 2006].

Heteromeric Slack-B/Slick channels also respond to PKC activation in a manner that is distinct from that of either subunit expressed alone: in fact, application of PKC activators in *Xenopus* oocytes expressing both subunits potently reduces currents by ~90%, an effect much greater than the degree of inhibition measured for homomeric KCNT2 channels.

- Modulation of KCNT1 and KCNT2 by G Protein-Coupled Receptors

KCNT1 and KCNT2 channel have been coexpressed in *Xenopus* oocytes with the M1 muscarinic receptor and the mGluR1 metabotropic receptor [Santi et al., 2006]. These are Gαq protein-coupled receptors that lead to the activation of PKC. The activation of these receptors leads to an increase in KCNT1 currents and a reduction of KCNT2 currents, consistent with the above mentioned effects prompted by a direct PKC activation. The importance of this regulation is suggested by a wide colocalization of these receptors with the SLO2 channel subunits throughout the nervous system.

- Modulation of SLO2 currents by cyclic AMP

Na^+-activated K^+ channels are also modulated by the biogenic amines such as dopamine (DA) and octopamine (OA), in an opposite way in Kenyon cells isolated from the

mushroom body of the cricket *Gryllus bimaculatus*.

In particular, in these cells OA and DA respectively increased and decreased the open probability of SLO2 channels. In addition, Na^+-activated K^+ channels are also modulated by cAMP/PKA (protein kinase A) signaling pathways leading to an increased channel open probability, and cGMP/PKG (protein kinase G) pathways responsible for a reduction in the open probability of SLO2 channels [Aoki et al., 2008].

The connexion between OA and cAMP-mediated signaling pathways is demonstrated by the fact the activation of OCTαR is also associated with a small increase in intracellular cAMP levels through the stimulatory G proteins (Gs), which in turn activate the protein Kinase A (PKA). In addition, insect dopamine receptors are G protein-coupled receptor (GPCR) and are classified into four subtypes: the D1-like dopamine receptors (Dop1), invertebrate dopamine receptors (INDRs, also known as Dop2), the D2-like dopamine receptors (Dop3) and the dopamine/ecdysteroid receptors (DopEcR). Once dopamine receptors are activated by dopamine, downstream signaling systems, such as the cyclic adenosine monophosphate (cAMP) or cyclic second messenger pathway and the inositol trisphosphate (IP3) second messenger pathway, are activated [Watanabe et al., 2013]. A possible connection between DA and cGMP has not yet been established.

- Modulation by PIP_2

A variety of ion channels has been shown to be regulated by phosphatidylinositol 4,5-biphosphate (PIP_2). The application of PIP_2 analogues (Dic8 $PI_{(3,4)}P2$ or Dic8 $PI_{(4,5)}P2$) on the cytoplasmic side increases the amplitude of KCNT1 and KCNT2 currents in *Xenopus* oocytes. Consistently, the exposure to pharmacological compounds, such as neomycin and wortmannin, that are able to reduce endogenous PIP_2 levels, induces a significant reduction of current amplitudes mediated by both channels [Tejada et al., 2012].

- Modulation by Estradiol

The open probability of KCNT1 and KCNT2 channels has been found to be increased by 17β-estradiol [Zhang et al., 2005].

- Interactions of KCNT1 channels with the Fragile X Mental Retardation Protein (FMRP)

The Fragile X syndrome is the most common inherited form of intellectual disability in humans. This syndrome is caused by a loss of expression of the RNA-binding protein FMRP (Fragile X mental retardation), also required for the normal activity-dependent protein translation in neurons. The cytoplasmic C-terminal domain of KCNT1 subunits interacts with FMRP that acts as a potent activator of KCNT1 channels. This protein-protein interaction is associated with the almost complete elimination of subconductance states. Furthermore, the application of a recombinant FMRP (1-298), which contains only the interaction domains of FMRP with KCNT1, reversibly increases the channel opening probability by two- to three-fold. On the other hand, FMRP was also found to have no effect on KCNT1 truncated channels (Slack-BΔ804), lacking sites essential for the interaction with FMRP [Brown et al., 2010].

1.7 Distribution of KCNT1 and KCNT2 channel subunits in the Central Nervous System (CNS)

Cloning of KCNT1 and KCNT2 genes and the development of specific antibodies have provided the unique opportunity to carry out a detailed study of the regional distribution of the encoded subunits. The highest levels of KCNT1 and KCNT2 channels have been found in the brain, with lower expression levels in the heart and kidney [Joiner at., 1998; Yuan et al., 2003; Bhattachaerjee and Kaczmarek, 2005]. KCNT2 is highly expressed in neurons, whereas no staining is found in glial cells. Strong hybridization was found throughout the brain, including the cerebral cortex, hippocampus, deep cerebellar nuclei, cerebellar Purkinje cells, reticular tegmental nucleus of the pons, preoptic nucleus, *substantia nigra*, and auditory brainstem nuclei [Joiner et al., 1998].

More recently, distribution pattern in the mouse brain of KCNT1 and KCNT2 channel subunits has been also described in more detail. The two channels exhibit distinct distribution, but their expression overlaps in some regions, including the olfactory bulb, subfornical organ, *substantia nigra*, *pars compacta*, oculomotor and red nuclei, interpeduncular and rhabdoid nuclei, nucleus of the trapezoid body, reticulotegmental nucleous of pons, and the inferior olivary complex. Several brain structures also exhibit expression pattern in which KCNT1 and KCNT2 do not overlap. In particular, KCNT1 immunoreactivity was found alone in islands of Calleja, nuclei of the extended amygdala, hippocampal formation, and ventromedial hypothalamic and arcuate nuclei. In contrast, a marked KCNT2 channel immunolabeling was found in *globus pallidus*, *substantia nigra*, pars reticulate and nigrostriatal bundle, and mesencephalic and parvicellular trigeminal nuclei and in parts of cerebellar cortex [Rizzi et al., 2016].

2. Role of Potassium channels in Epilepsy

Potassium (K^+) channels underlie outward K^+ currents that contribute to membrane repolarization and hyperpolarization, thus limiting the neuronal excitability. Such channels are the only ion-selective cation channels that have an equilibrium potential near the typical cellular resting potential.

Potassium channels are expressed in almost every cell, particularly in neurons and excitable tissues, where they regulate the shape and duration of action potentials, the firing rate and the overall excitability of cells. The functional heterogeneity of K^+ currents expressed in excitable and non-excitable cells is primarily due to the large number of genes either encoding pore-forming (α) or accessory (β) subunits in the mammalian genome. Additional factors, such as alternative splicing, RNA editing, and ability to form homomeric or heteromeric complexes among pore-forming and accessory subunits also contribute to the K^+ channel properties diversification and expression levels. More than 80 genes encoding for K^+ channels have been cloned representing the largest group of ion channels regulating the electrical activity of cells in different tissues. It is therefore not surprising that mutations in these genes leading to ion channels dysfunctions cause several diseases and, in particular, epilepsy in humans and animal models [Villa and Combi, 2016].

Epilepsies are common neurological disorders in infancy, childhood and adolescence characterized predominantly by recurrent and unpredictable interruptions of normal brain function, called epileptic seizures (Fisher et al., 2005).
According to the International League Against Epilepsy (ILAE), an epileptic seizure is “a transient occurrence of signs and/or symptoms due to abnormal excessive or synchronous neuronal activity in the brain”.
The definition of epilepsy also implies the occurrence of at least one epileptic seizure, where the term “seizure” indicates an “abnormal and synchronous excitation of a neuronal population lasting seconds or minutes”.
Epileptic seizures arise when functional alterations of neurons occur, causing an excessive and transient discharge of action potentials. Since the epileptic seizure can

involve a specific neuronal population or the whole brain, the semiology of the epileptic seizures varies according to the neuronal populations and/or cerebral circuits involved.

Generally, seizures arise when there is a disruption of the mechanisms controlling the physiological balance between neuronal excitation and inhibition. Cell membrane of neurons have several different ion channels, including Na^+ and K^+ leak channels as well as voltage-gated Na^+ and K^+ channels that allow the passage of ions as a function of their electrochemical gradients. Cl^- and Na^+ are mainly located in the extracellular fluid, while K^+ ions and negatively charged proteins are located in the intracellular fluid therefore K^+ ions leak out of the cell, moving down their concentration gradient. As K^+ leaves the cell, the negatively charged proteins are unable to follow because the cell membrane is not permeable to them.

The loss of positive ions from the cell creates an electrical gradient. Because opposite charges attract each other, the negative proteins inside the cell try to pull K^+ back into the cell. At some point in this process, the electrical force attracting K^+ into the cell becomes equal in magnitude to the chemical concentration gradient driving K^+ out of the cell. At that point, called equilibrium potential for K^+ (-90 mV), net movement of K^+ across the membrane stops. By contrast, because Na^+ is more concentrated outside the cell, some Na^+ ions moves into the cell and accumulates there until the equilibrium potential for Na^+ (+60 mV) as most cells are about 40 times more permeable to K^+ than to Na^+ cell membrane resting potential is closer to the K^+, rather than Na^+ equilibrium potential (-90 mV).

Therefore it is plausible that abnormalities in Na^+ or K^+ channel function can dramatically alter neuronal firing, through different mechanism depending on the possibility that specific classes of ion channels are expressed in inhibitory and/or excitatory neurons.

The concept that an alteration of the balance between excitation and inhibition processes is responsible for the onset of epileptic seizures has led to the design of anticonvulsant drugs able to restore the physiological neuronal excitability. The traditional antiepileptic drugs, in fact, act mainly through inhibition of Na^+ (phenytoin, carbamazepine, lamotrigine) or Ca^{2+} (ethosuximide) channels or by increasing the

inhibitory GABAergic transmission (phenobarbital, benzodiazepines, tiagabine, vigabatrin).

The etiology of epilepsy is very heterogeneous: many different genetic and pathophysiological factors, alone or in combination, can underlie an increased risk of developing a seizure disorder [Berg et al., 2010].

The contribution of **genetic factors** is observed when the epileptic seizures are the direct result of a known or presumed genetic defect. Also, genetic causes can be heterogeneous: in fact, epilepsy-causing mutations have been identified in different genes; in addition, these mutations can be inherited, can occur *de novo* in the affected individuals, or in rare case can consist in chromosomal abnormalities (e.g., trisomy 21). The assignment of the disorder as genetic does not exclude the possibility that environmental factors may contribute to the expression of disease.

Epilepsy may be also related also to **structural** or **metabolic** causes: lesions, such as those induced by trauma, stroke, infection, or cerebral tumors, may be associated to a substantially increased risk of developing epilepsy. They may also be of genetic origin as it occurs for tuberous sclerosis.

In some cases, the nature of underlying cause is **unknown** or is the consequence of a separate unrecognized disorder.

2.1 The Epileptic Encephalopathies: an overview

One third of the epilepsies is refractory to medical treatments, and an important fraction of them have a significant detrimental effect on cognitive and brain functions. These conditions in which the epileptic activity during brain maturation is the main causative factor of severe cognitive and behavioral impairments, are referred to as **epileptic encephalopathies (EEs)**, a group of devastating epileptic disorders that occur early in life and are often characterized by drug resistance, persistent severe electroencephalographic abnormalities, cognitive dysfunction or decline with poor developmental outcome [Scheffer et al., 2017]. The etiologies of an encephalopathy are heterogeneous and the brain dysfunction can occur either acutely or chronically and can be static or degenerative [Helbig et al., 2017]. Refractory seizures, severe EEG

abnormalities, and developmental delay/regression or intellectual disability are the three main features of EEs.

2.2 The Genetics of the Epileptic Encephalopathies

The current genetic landscape and functional framework in which the epileptic encephalopathies exist were established by stages of gene discovery that occurred over the last 15 years (Figure 5). At the beginning, in the era of family studies, the first genes for familial epilepsies were discovered by systematic analysis of large families with mild dominant epilepsies. These findings, including the discoveries of *CHRNA4*, *SCN1A*, *SCN1B*, *KCNQ2* and *GABRG2*, laid the foundation for the channelopathy concept of human epilepsies [Steinlein et al., 1995; Singh et al., 1998; Claes et al., 2001; Sugawara et al., 2002].

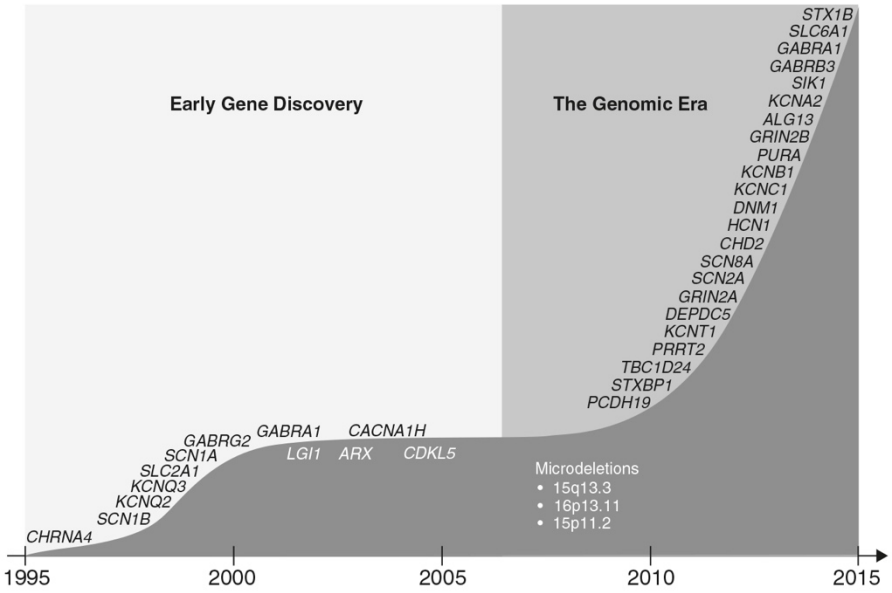

Figure 5 Gene discovery in human epilepsies [Helbig et al., 2017]

The initial era of gene discovery from large epilepsy families was followed by a period of relative stagnation when very few novel genes were identified. Only in recent years, the advent of large-scale next generation sequencing technologies has strongly increased the speed of gene discovery, leading to the identification of a growing number of ion

and non-ion-channels genes in sporadic severe and treatment-resistant epileptic encephalopathies (Table 2). An important contribution to the identification of novel genes responsible for Epileptic Encephalopathies has been given by new genetic technologies for mutation detection in human genome, such as Next-Generation Sequencing (NGS) and/or Whole Exome Sequencing (WES) [Choi et al., 2009]. The NGS technology, also known as "massive parallel sequencing", has largely replaced traditional Sanger sequencing in the research and clinical laboratories allowing the simultaneous sequencing of millions of short fragments of DNA. The NGS technology is rapidly becoming a fundamental tool for genetic and functional genomics, since this technique allows the sequencing of entire gene panels, ranging from a few to several hundred genes. In addition, advances in genome technologies have allowed WES, in which the exon sequence of nearly all ~ 2000 human genes are sequenced in order to identify genetic mutations [Mefford, 2015]. Each of these approaches has been fundamental for the discovery that about 75% of patients with epileptic encephalopathies have *de novo* mutations, with only a small subset of patients with dominant, recessive or X-linked inherited mutations [Helbig et al., 2016]. Application of NGS technologies has also strongly contributed to demonstrate the significant genetic heterogeneity of EEs, as summarized in Table 2.

OMIM	Gene	Mode of Inheritance	Protein
EIEE1	*ARX*	XL	Homeobox protein ARX
EIEE2	*CDKL5*	XL	Cyclin-dependent kinase-like 5
EIEE3	*SLC25A22*	AR	Mitochondrial glutamate carrier 1
EIEE4	*STXBP1*	AD	Syntaxin-binding protein 1
EIEE5	*SPTAN1*	AD	Spectrin alpha chain, non-erythrocytic 1
EIEE6	*SCN1A*	AD	Sodium channel protein type 1 subunit alpha
EIEE7	*KCNQ2*	AD	Potassium voltage-gated channel subfamily KQT member 2
EIEE8	*ARHGEF9*	XL	Rho guanine nucleotide exchange factor 9
EIEE9	*PCDH19*	XL	Protocadherin-19
EIEE10	*PNKP*	AR	Bifunctional polynucleotide phosphatase/kinase
EIEE11	*SCN2A*	AD	Sodium channel protein type 2 subunit alpha
EIEE12	*PLCB1*	AR	1-phosphatidylinositol 4,5-bisphosphate phosphodiesterase β-1
EIEE13	*SCN8A*	AD	Sodium channel protein type 8 subunit alpha
EIEE14	***KCNT1***	**AD**	**Potassium channel subfamily T member 1**
EIEE15	*ST3GAL3*	AR	CMP-N-acetylneuraminate-β-1,4-galactoside α-2,3-sialyltransferase
EIEE16	*TBC1D24*	AR	TBC1 domain family member 24
EIEE17	*GNAO1*	AD	Guanine nucleotide-binding protein G(o) subunit alpha
EIEE18	*SZT2*	AR	Protein SZT2
EIEE19	*GABRA1*	AD	Gamma-aminobutyric acid receptor subunit alpha-1
EIEE20	*PIGA*	XL	Phosphatidylinositol N-acetylglucosaminyltransferase subunit A
EIEE21	*NECAP1*	AR	Adaptin ear-binding coat-associated protein 1
EIEE22	*SLC35A2*	XL	UDP-galactose translocator
EIEE23	*DOCK7*	AR	Dedicator of cytokinesis protein 7
EIEE24	*HCN1*	AD	Potassium/sodium hyperpolarization-activated cyclic nucleotide-gated channel 1
EIEE25	*SLC13A5*	AR	Solute carrier family 13 member 5
EIEE26	*KCNB1*	AD	Potassium voltage-gated channel subfamily B member 1
EIEE27	*GRIN2B*	AD	Glutamate receptor ionotropic, NMDA 2B
EIEE28	*WWOX*	AR	WW domain-containing oxidoreductase
EIEE29	*AARS*	AR	Alanine--tRNA ligase
EIEE30	*SIK1*	AD	Serine/threonine-protein kinase SIK1
EIEE31	*DNM1*	AD	Dynamin-1
EIEE32	*KCNA2*	AD	Potassium voltage-gated channel subfamily A member 2
EIEE33	*EEF1A2*	AD	Elongation factor 1-alpha 2
EIEE34	*SLC12A5*	AR	Solute carrier family 12 member 5
EIEE35	*ITPA*	AR	Inosine triphosphate pyrophosphatase

Table 2 Early-Infantile-Epileptic-Encephalopaties (EIEEs) associated genes; XL=x-linked, AR=autosomal recessive, AD=autosomal dominant [Gene review. *Miceli et al. 2016*]

2.3 KCNT1 mutations result in a wide range of seizure disorders and Intellectual Disabilities

Mutations in KCNT1 gene have been identified in widely-diverging clinical conditions, ranging from very severe form of epilepsy (MMPSI) to milder epileptic diseases (ADNFLE) [Lim et al., 2016]. *In vitro* functional studies revealed that all KCNT1 mutations are able to induce an increase in current density when compared to wild-type channels, a result referred to as gain-of-function effect. In contrast, only one single study has reported a KCNT1 mutation causing a reduction in channel activity, also referred to as loss-of-function effect [Evely et al., 2017].

Clinical features of most epileptic conditions associated to KCNT1 mutations are described below.

2.3.1 Malignant Migrating Partial Seizures of Infancy

The syndrome of Malignant Migrating Partial Seizures of Infancy (MMPSI) or EIEE14 (Early Infantile Epileptic Encephalopathy 14) is a severe form of epilepsy that begins very early in life. Recurrent seizures begin before the age of 6 months, but commonly start within a few weeks after birth. Although affected patients may develop normally at first, progression stalls and skills decline when seizures begin; as a result, affected individuals have profound developmental delay. The seizures in MMPSI are described as partial (or focal) because seizure activity occurs in specific regions of the brain rather than affecting the entire brain. Seizure activity may appear in multiple locations of the brain or move, hence the definition of migrating seizures, from one brain region to another during an episode (Figure 6).

Migrating focal motor seizures at onset, nearly continuous multifocal seizures migrating between cortical regions and hemispheres, resistance to antiepileptic drugs, lack of demonstrable etiology, and severe psychomotor delay on follow-up are typical in MMPSI patients [Coppola et al., 1995].

The natural history of this syndrome allows recognition of three distinct phases. A first phase, generally starting in the first semester after birth, is often characterized by sporadic seizures, usually recurring in a few weeks or months. Seizure onset may also occur since the first day of life [Hmaimess et al., 2006]. Seizures are mainly focal motor

with rapid secondary generalization; autonomic manifestations such as apnea, flushing, or cyanosis frequently occur. This phase usually lasts a few weeks or months. However, seizures sometimes occur at the onset of the second phase. Interictal electroencephalography (EEG) in this first period shows increasing diffuse slowing of background activity with prevalence of slow waves often shifting from one hemisphere to the other. Shortly, multifocal discharges poorly activated by sleep are present in all cases.

The second phase could also be defined as a ‘‘stormy phase.’’ At an age ranging from about 1–12 months, focal polymorphous seizures shortly become very frequent, occurring in clusters of 5–30 several times a day or being almost continuous for several days. With increasing age, the amplitude of the ictal discharge tends to increase, and frontal areas are more frequently affected [Dulac, 2005]. The age at onset of the third phase may vary highly, ranging from the end of the first year to 5 years of age and over. This phase is a relatively seizure-free period, although spontaneous intercurrent illnesses would easily trigger clusters of seizures or occasional status epilepticus.

Computed tomography (CT) and magnetic resonance imaging (MRI) are generally normal at the beginning of the illness. During follow-up, there may be a mild to moderate enlargement of both subarachnoid and ventricular spaces.

Overall, the long-term outcome of migrating focal seizures in infancy, with reference to seizures and psychomotor development, remains very severe. Even when it becomes possible to shorten the duration of migrating status epilepticus and/or increase the intervals between active phases with different combination therapies, psychomotor abilities are poor, inevitably evolving into mental retardation. Not surprisingly, absence of language and hypotonia are also commonly noted in MMPSI patients [McTague et al., 2013]. Because of the serious health problems caused by MMPSI, many affected individuals do not survive past infancy or early childhood.

Possible causes for seizure development in MMPSI patients has remained elusive until recently. Neurometabolic, blood gas and serum tests are typically normal, and brain lesions are rarely observed in affected patients [Nabbout and Dulac, 2008]. Genetic etiologies for MMPSI were first identified in 2011, with the discovery of SCN1A (Nav 1.1)

mutations [Carranza Rojo et al., 2011], followed by TBC1D24 [Milh et al., 2103] and KCNT1 (Slack) mutations [Barcia et al., 2012].

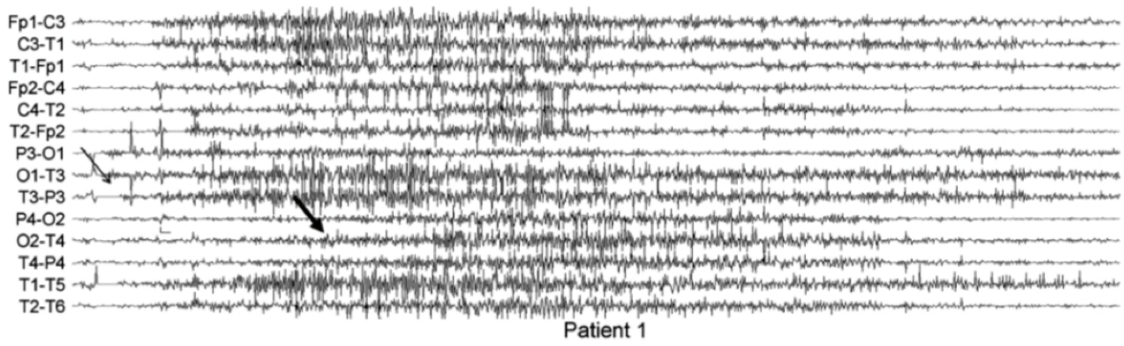

Figure 6 Ictal EEG of a MMPSI patients. Ictal focus is located in the left temporal area at the onset (narrow arrow), whereas it is shifted to the right occipital area during seizure (broad narrow). [Ishii et al., 2013].

2.3.2 Ohtahara syndrome

Ohtahara syndrome (OS) was originally described as an early infantile epileptic encephalopathy with suppression bursts [Ohtahara et al., 1976]. OS is one of the earliest seizures in its presentation. Infants acutely develop tonic spasms that can be either generalized or lateralized, can occur both singly or in clusters, and are independent of the sleep cycle. A majority of OS patients show severe developmental delay, including intellectual disability. More than 80% of OS patients reported in the literature have a developmental delay, while only 10% are described as showing normal development. It remains a challenge to reverse or overcome this poor prognosis, since these seizures have pronounced pharmacological resistance [Beal et al., 2012]. Genetic etiologies have also been identified in a subset of OS patients. To date, alterations in five genes have been found in OS patients: ion channels *KCNQ2* (Kv7.2) [Saitsu et al., 2012a], *SCN2A* ($Na_v1.2$) [Nakamura et al., 2013], *KCNT1* (Slack) [Martin et al., 2014]; the transcription factors ARX and the synaptic binding protein STXBP1. Approximately one third of patients with Ohtahara syndrome will also develop other seizure types, most commonly focal motor seizures, hemiconvulsions, or generalized tonic-clonic seizures. OS may evolve to West syndrome and further to Lennox-Gastaut syndrome during age progression with a poor prognosis.

2.3.3 Early Myoclonic Encephalopathy

Similar to OS, the pathogenesis of early myoclonic encephalopathy (EME) is variable, with structural, metabolic, and genetic abnormalities all playing a role. Many seizure types may occur, but myoclonic seizures (very frequent, brief, single or repetitive, erratic, and nearly continuous body jerks) characterize this epilepsy syndrome and differentiate it from OS. Some may also have focal motor seizures, tonic seizures, or rarely tonic spasms, which appear later. ErbB4 is one gene example associated with EME [Backx et al., 2009], although mutations in SLC25A22 gene have reported in patients with EME [Molinari et al., 2005].

2.3.4 West Syndrome

West syndrome (WS) is the most common form of early onset epileptic encephalopathy and typically begins between 3 and 7 months of age. WS is characterized by epileptic spasms, hypsarrhythmia and developmental cessation or regression. The epileptic spasms typical of WS are brief seizures with flexion or extension of the arms and legs and/or head and torso that occur in clusters usually upon awakening [Nieh et al., 2014].

2.3.5 Autosomal dominant nocturnal frontal lobe epilepsy

Autosomal dominant nocturnal frontal lobe epilepsy (ADNFLE) is characterized by clusters of nocturnal motor seizures, which are often stereotyped and brief (5 seconds to 5 minutes). They vary from simple arousals from sleep to dramatic, often bizarre, hyperkinetic events with tonic or dystonic features. Affected individuals may experience aura. Retained awareness during seizures is common. A minority of individuals experience daytime seizures. Onset ranges from infancy to adulthood. About 80% of individuals develop ADNFLE in the first two decades of life; mean age of onset is ten years. Clinical neurologic examination is normal and intellect is usually preserved, but reduced intellect, psychiatric comorbidity, or cognitive deficits may occur. Within a family, the manifestations of the disorder may vary considerably. ADNFLE is lifelong but not progressive. As an individual reaches middle age, attacks may become milder and

less frequent. Molecular genetic testing reveals pathogenic variants in CHRNA4, CHRNB2, CHRNA2, KCNT1, DEPDC5, or CRH in approximately 20% of individuals with a positive family history and fewer than 5% of individuals with a negative family [Kurahashi et al., 2015].

3. Pharmacology of Sodium-activated potassium channels

Given their role in the regulation of neuronal excitability and their involvement in the pathogenetic mechanisms of several epileptic disorders, these sodium-activated potassium channels are important pharmacological targets.

The pharmacological properties of KCNT1 and KCNT2 channels are similar to each other, but differ from those of many other potassium channels. In fact, KCNT1 and KCNT2 channels are only weakly sensitive to the aspecific potassium channel blocker **tetraethylammonium (TEA):** in particular, 1 mM TEA had little effect on both channels while a concentration of 20 mM was required to block 60% of KCNT1 and KCNT2 currents. In addition, **Ba^+** (1 mM), another aspecific K^+ channels blockers, also inhibited KCNT1 and KCNT2 channels with time- and voltage-dependent effects [Bhattacharjee et al., 2003].

Studies on native I_{KNa} channels in cardiac cells indicate that several antiarrhythmic drugs inhibit KCNT1 and KCNT2 channels in cardiac cells [Mori et al., 1996; Li et al., 1999]. Some of these compounds, such as **clofilium, bepridil,** and **quinidine** (Figure 7), have been also found to be very effective and reversible blockers of KCNT1 and KCNT2 currents expressed in oocytes and mammalian cells. Clofilium inhibits both channels and this compound seems to be more potent on KCNT1 channels: in fact, the EC_{50} for KCNT1 is 109 μM, while the EC_{50} for KCNT2 is 331 μM [Tejada et al., 2012]. Two other blockers, namely bepridil and quinidine, inhibit KCNT1 currents in a concentration-dependent manner and decrease channel activity in excised membrane patches. Similarly to oocytes, the application of quinidine (1 μM-10 mM) in HEK293 cells expressing KCNT1 produced a rapid decrease in current amplitude, with an EC_{50} of 89.6 μM [Yang et al., 2006]. The KCNT1 currents are also sensitive to bepridil-induced blockade, with the latter being more potent than quinidine (EC_{50} of 1.0 μM) [Yang et al., 2006]. Although these drugs are able to block K_{Na} channels, they are also active on a variety of other channel types, thus rendering difficult the identification of their precise mechanism of action during their clinical use.

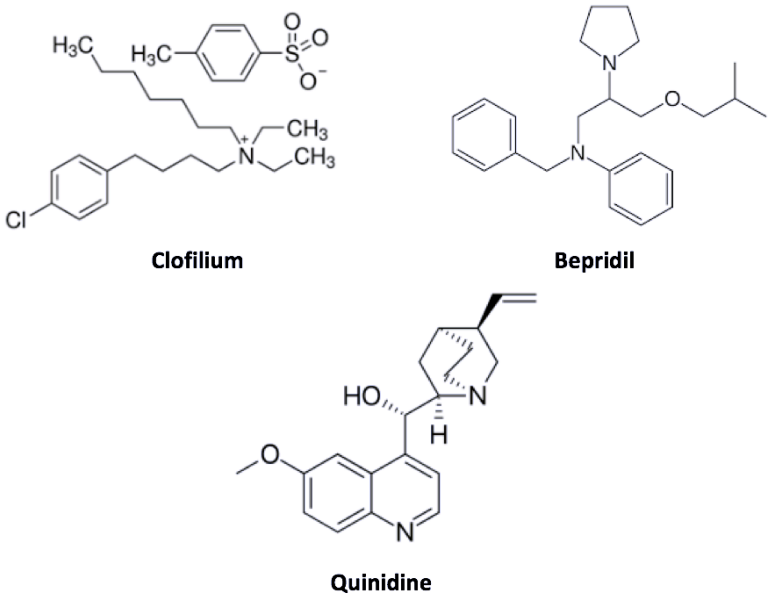

Figure 7 Chemical structure of KCNT1 and KCNT2 blockers.

A variety of compounds that **activate** SLO2 K^+ channels are also known. The first to be described was the bis-phenol anti-parasitic compound bithionol, which in KCNT1-expressing HEK cells produces a robust increase in current amplitude, whit an EC_{50} of 0.77 μM [Yang et al., 2006]. Similar bithionol-induced current increases are observed in KCNT1-expressing oocytes and for native K_{Na} currents in neurons of the auditory brainstem. Bithionol reversibly activates KCNT1 channels even when applied to the extracellular face of excised patches; however, bithionol is not selective for K_{Na} channels because it also activates SLO1 calcium-activated potassium channels [Yang et al., 2006; Yang et al., 2007]. A screen of pharmacologically active compounds using a rubidium flux assay against KCNT1 channels expressed in Chinese Hamster Ovary (CHO) cells has revealed new activators: these include **riluzole**, **loxapine**, an antipsycotic agent, and **niclosamide**, an anthelmintic agent (Figure 8). Loxapine was found to be more selective than bithionol since no effects on SLO1 calcium-activated potassium channels were observed. Electrophysiological experiments revealed that loxapine is effective on recombinant human and rat KCNT1 channels and that it activates native K_{Na} channels in isolated DRG neurons [Biton et al., 2012].

Furthermore, KCNT2 channels can be activated by fenamates such as niflumic acid (NFA, Figure 6), even in the absence of intracellular Na^+. In *Xenopus oocytes*, KCNT2

currents were rapidly activated by extracellular application of NFA (EC_{50} 2.1 mM) or flufenamic acid (EC_{50} 1.4 mM) [Dai et al., 2010].

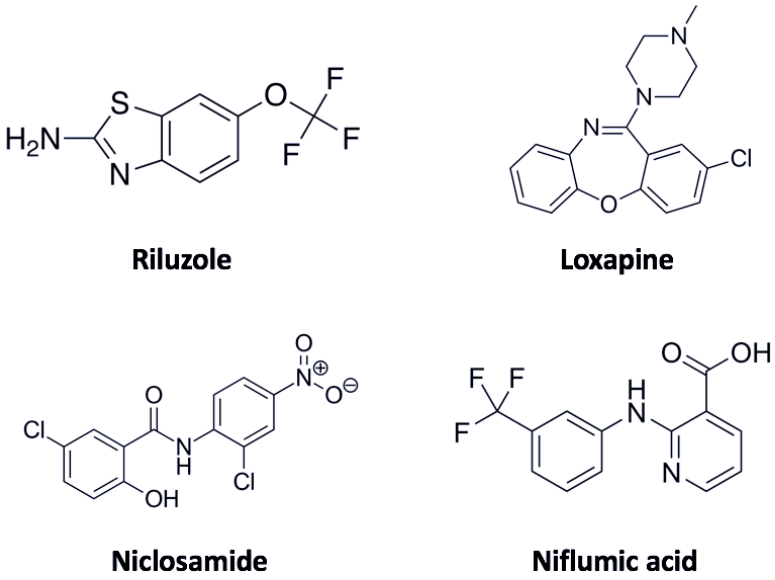

Figure 8 Chemical structure of KCNT1 and KCNT2 activators.

4. AIMS OF THE STUDY

Epilepsy has a highly heterogeneous etiology with a strong genetic contribution. In particular, mutations in the KCNT1 gene cause a wide spectrum of seizure phenotypes including ADFNLE, multifocal epilepsy, Ohtahara syndrome, leukoencephalopathies and the rare devastating epileptic encephalopathy MMPSI.

However, the identification of one of the many various gene variants identified in each patient with state-of-the-art technologies as pathogenic, requires the convergence of data deriving from various sources. Among these, functional, pharmacological and biochemical *in vitro* studies are essential to understand the pathogenetic contribution of a specific variant found in patients affected by this severe genetic disease. Therefore, in order to facilitate the identification of specific gene variants as pathogenic in specific individuals affected by rare epileptic conditions, and to provide clues on the potential pathogenetic mechanisms, in the present Doctoral Thesis, I have investigated the biochemical, functional, and pharmacological properties of KCNT1 and KCNT2 channels carrying mutations identified in patients affected by Epileptic Encephalopathy. The genetic variants investigated in the present study are listed in following Table:

Gene	Nucleotide substitution	Amino acids substitution	Reference
KCNT1/SLO2.2	c.862 G>A	p. G288S	Ishii et al., 2013 [Rizzo et al., 2016]
KCNT1/SLO2.2	c.1546 A>G	p. M516V	[Rizzo et al., 2016]
KCNT1/SLO2.2	c.2677 G>A	p. E893K	newly-identified
KCNT1/SLO2.2	c.2849 G>A	p. R950Q	Moller et al., 2016
KCNT2/SLO2.1	c.1451 G>A	p. C484Y	newly-identified
KCNT2/SLO2.1	c.569 G>C	p. R190H	newly-identified
KCNT2/SLO2.1	c.569 G>C	p. R190P	[DDDS, Nature 2017]

Table 3 Naturally-occurring mutations found in KCNT1 and KCNT2 genes studied in the present doctoral thesis. ("c." indicates nucleotide substitutions, "p." indicates amino acid mutations).

In particular, I have studied four mutations (G288S, M516V, E893K and R950Q) in the KCNT1 gene and three mutations (C484Y, R190H and R190P) in the KCNT2 gene. Among them, two KCNT1 mutations (G288S and R950Q) have already been reported in the literature [Ishii et al., 2013; Moller et al., 2015]. The identification of KCNT1 mutations has been made possible thanks to collaboration with a multidisciplinary team formed by child neurologists and human geneticists. Two MMPSI-affected patients have been identified by Prof. G. Coppola, who described this disease for the first time [Coppola et al., 1995], dr. G. Casara (Department of Pediatrics, Regional Hospital of Bolzano), and dr. M. Vecchi (Department of Child and Mother Health, University of Padua); in these patients, the genetic analysis performed by the group of Prof. A. Weisz (University of Salerno) identified the recurrent KCNT1-G288S and the novel KCNT1-M516V mutations. In addition, the novel KCNT1-E893K variant has been identified by the group of dr. J. DiFrancesco at the "Carlo Besta" Institute, while the recurrent KCNT1-R950Q variant has been found in a patient by dr. R. Dilena (Fondazione IRCSS Ca Granda Ospedale Maggiore Policlinico, Milan).

As reported in Figure 9, M516V, E893K and R950Q mutations affect residues localized in the KCNT1 C-terminal region: M516V falls within the RCK1 domain, whereas E893K and R950Q are localized in the RCK2 domain; by contrast, G288S falls in the S_5 segment of the KCNT1 channel subunit.

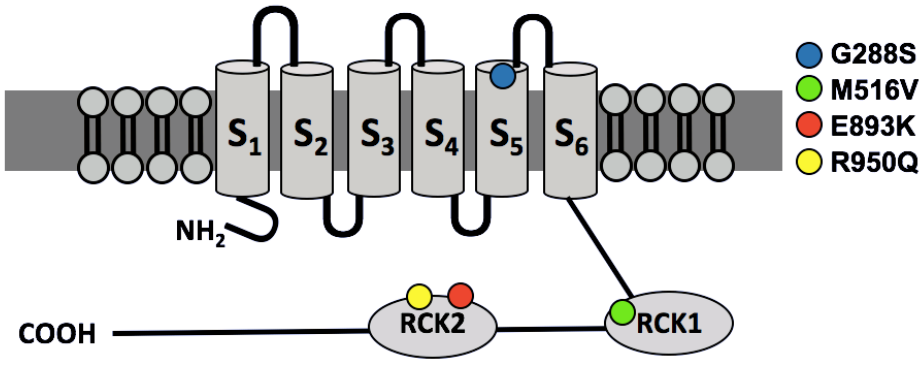

Figure 9 Schematic topology of a KCNT1 (SLO2.2) channel subunit and location of the mutations studied in the present work. Colored circles indicate the location of the mutations investigated: the G288S mutation (blue circle) is localized in the S_5 segment of the channel, while the other mutations are located in the C-terminal region. The M516V mutation (green circle) fall in the RCK1 (Regulator of K^+ conductance) domain of the KCNT1 subunits, while the E893K (red circle) and R950Q (yellow circle) mutations are localized in the RCK2 domain. For numbering mutations, numeration complies with that of isoform 2 (NM_020822).

Also KCNT2 mutations herein investigated have been identified through a network of collaboration in Italy and abroad: in particular, the KCNT2-R190H variant has been identified in collaboration with the Prof. Johannes Lemke (Germany), while the KCNT2-R190P variant was recruited through the Deciphering Developmental Disorders Study [DDDS, Nature 2017]. In addition, I have also investigated the functional consequences of another variant in KCNT2 (C484Y) found in a patient with Autosomal Dominant Nocturnal Frontal Lobe Epilepsy (ADFNLE) and identified by Prof. Francesca Bisulli (University of Bologna); this variant has been inherited from father's patient. As shown in Figure 10, the C484Y mutation falls within the C-terminal region of the KCNT2 subunit, while both mutations affecting the same residue (R190H and R190P) are located in the S_4-S_5 linker region.

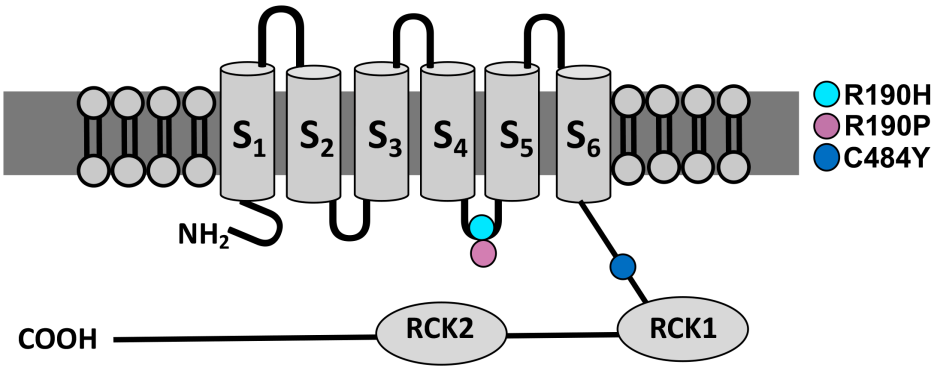

Figure 10 Schematic topology of a SLO2.1 channel subunit and location of the mutations studied in the present work. Colored circles indicate the location of mutations investigated: *de novo* R190H and R190P mutations are localized within the S_4-S_5 linker region, while the inherited C484Y mutation is located in the C-terminal region of the KCNT2 channel subunit. For numbering mutations, the numeration complies with that of isoform *NM_001287820.2.*

To study the biochemical, functional, and pharmacological consequences prompted by these mutations in SLO2 family genes, the following experiments have been performed:

a) for KCNT1 mutations:

1. engineering of each mutation in a plasmid containing the cDNA for a myc-DDK tagged human isoform of KCNT1 (RC214820; Origene, Rockville, MD, USA);
2. patch-clamp recordings of macroscopic currents from Chinese Hamster Ovary (CHO) cells transiently-transfected with wild-type or mutant subunits, in homomeric or heteromeric configurations with wild-type and mutant KCNT1 subunits;
3. biochemical evaluation of total and plasma membrane expression of wild-type and mutant KCNT1 subunits;
4. patch-clamp recordings of macroscopic currents in the presence of two well-known KCNT1 blockers (bepridil and quinidine) in order to evaluate their ability to restore the functional alterations induced by the presence of each mutation.

b) for KCNT2 mutations:

1. engineering of mutations in a plasmid containing the cDNA for a turbo-GFP tagged human isoform of KCNT2 (RC216225; Origene, Rockville, MD, USA);
2. biochemical studies by using CHO or HEK-293 total lysates in order to identify the most efficient heterologous expression system for KCNT2 subunits;
3. patch-clamp recordings of macroscopic currents from Human Embryonic Kidney (HEK-293) cells transiently-transfected with wild-type or mutant subunits, in homomeric or heteromeric configurations with wild-type and mutant KCNT2 subunits;
4. patch-clamp recordings of macroscopic currents in the presence of the KCNT2-blocker quinidine in order to evaluate its ability to restore the functional alteration induced by the presence of each mutation;
5. molecular modelling studies to formulate hypothesis on the potential structural consequences of the R190 variants.

5. MATERIALS AND METHODS

5.1 Site-Directed Mutagenesis

Each KCNT1 mutation was engineered by Quick-change Site-Directed Mutagenesis (*Agilent Technologies*) in a pCMV6-KCNT1 *(RC214820; Origene, Rockville, MD, USA)* plasmid containing the cDNA for myc-DDK tagged human transcript variant of KCNT1 (accession number: NM_020822; 1256 aminoacids).

Similarly, mutations in KCNT2 gene were obtained by Quick-change Site-Directed Mutagenesis in a pCMV6-KCNT2 plasmid *(RG216225; Origene, Rockville, MD, USA)* encoding for the tGFP-tagged human transcript variant of KCNT2 (accession number: NM_198503; 1135 aminoacids).

The mutations were engineered in each plasmid by Polymerase Chain Reaction (PCR), using a pair of primers (forward and reverse), incorporating the nucleotide mutation found in each patient (see Table 4).

Mutation	Template	Primers
c.862 G>A; p. G288S	KCNT1 100 ng	5'-GACCTGC**A**GCATCCAGCAC-3' 3'-GTGCTGGATGC**T**GCAGGTC-5'
c.1546 A>G; p. M516V	KCNT1 100 ng	5'-GTACGCCGT**G**CTGGCGC-3' 3'-GCGCCAG**C**ACGGCGTAC-5'
c.2677 G>A; p. E893K	KCNT1 100 ng	5'-CCGAG**A**AGGACTACATG -3' 3'-CCATGTAGTCCT**T**CTCGG-5'
c.2849 G>A; p. R950Q	KCNT1 100 ng	5'-GGGAGC**A**AGAGAATGGC-3' 3'-GCCATTCTCT**T**GCTCCC-5'
c.1451 G>A; p. C484GY	KCNT2 200 ng	5'-GGTAGATACTCCGGGAATG-3' 3'-CATTCCCGGAGTATCTACC-5'
c.569 G>A; p. R190H	KCNT2 200 ng	5'-CATTCAGC**A**TACACAGTCTG -3' 3'-CAGACTGTGTA**T**GCTGAATG -5'
c.569 G>C; p. R190P	KCNT2 200 ng	5'-CATTCAGC**C**TACACAGTCTG -3' 3'-CAGACTGTGTA**G**GCTGAATG -5'

Table 4 Experimental conditions used for PCR reaction. Column 1 indicates the mutations found in patients affected by Epileptic Encephalopathy. Column 2 shows the templates and related quantity used for each reaction. Column 3 contains nucleotide sequences of primers used for PCR reaction.

The amplification reaction was performed in a final volume of 50 µL containing the following components: 100-200 ng of plasmids for wild-type KCNT1 or wild-type KCNT2 as template, 0.6 µM primer forward, 0.6 µM primer reverse, 3U of Q5 DNA Polymerase, 0.2 mM dNTP mix, 1X buffer Q5 and 1X buffer GC. The PCR consisted of 30 cycles, with each cycle consisting of three temperature steps, that allow the denaturation of the DNA double helix (95° C for 1'), the annealing of the primers to the single strand of DNA (the temperature was modified according to the nucleotide sequence of each couple of primers) and the extension of the primers (73°C for 5') (Figure 11).

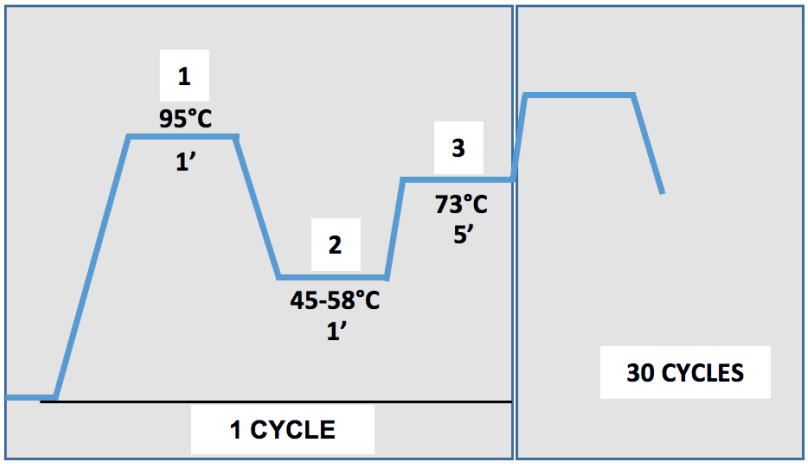

Figure 11 Polymerase Chain Reaction (PCR) protocol. PCR protocol consists of 3 phases. Phase 1: denaturation of the DNA. Phase 2: annealing of the mutated primers to specific complementary region of the DNA. Phase 3: The Q5 polymerase synthesizes a new DNA strand complementary to the DNA template strand.

5.2 Bacterial Transformation and plasmidic DNA preparation

The amplification reaction contains both methylated (parental) and unmethylated (neo-synthesized) DNA. In order to remove the parental DNA, the entire volume reaction was exposed to enzymatic digestion with DpnI enzyme, able to digest only methylated DNA.

After the enzymatic digestion with DpnI, competent *E.coli* DH5α cells were transformed with the PCR product by chemical transformation procedure (30' at 4°C, shock step at 42° for 45'' followed by 2' at 4°C). To help the bacterial cells to recover from the heat shock, cells were incubated with SOC medium (2% tryptone, 0.5% yeast extract, 10 mM

NaCl, 2.5 mM KCl, 10 mM $MgCl_2$, 10 mM $MgSO_4$, 20 mM glucose), for 1h at 37°C. After this step, the cells were seeded into LB+agar plates (containing 10g/L tryptone, 5 g/L yeast extract, 5 g/L NaCl, agar 15 g/L) containing the specific antibiotic to which plasmids are resistant (in our experiments ampicillin 100 μg/μL) to allow the selective growth of *E.coli* cells transformed with myc-DDK pCMV6-KCNT1 or tGFP-pCMV6-KCNT2. Plates were then incubated upside down at 37°C for about 17h to allow bacterial growth.

Each colony grown on the LB medium was inoculated in 6 mL of fresh LB medium with ampicillin for selection, at 37°C/220 rpm overnight. Plasmidic DNA was extracted by using a commercially available kit *(NucleoSpin Plasmid EasyPure, Promega, Milan, Italy).* The successful insertion of each desired mutation was verified by direct sequencing *(Eurofins Genomic, Milan, Italy)*. In order to obtain a large amount of DNA, one of the positive clones, was amplified on a large scale (500 mL) and plasmidic DNA was obtained by using a commercially available kit *(PureYield Plasmid Maxiprep System, Promega)*. The cDNA was sequenced to confirm the presence of the mutation of interest and to exclude the presence of additional mutations in the coding sequence.

5.3 Cell cultures and transient transfection with Lipofectamine 2000

CHO (Chinese Hamstery Ovary) or HEK-293 (Human Embryonic Kidney) cells were grown in plastic Petri's dishes (100 mm, 60 mm or 40 mm, according to the different experimental procedures) in DMEM *(Dulbecco's Minimum Eagle Medium)* supplemented with 10% Fetal Bovine Serum (FBS) decomplemented at 56°C for 30', 1% L-glutamine (2 mM in 0.85% NaCl), 1% penicillin (50 U/mL) and streptomycin (50 μg/mL) in a humidified atmosphere at 37°C with 5% CO_2. The CHO cells were transiently transfected using Lipofectamine 2000, according to the manufacturer protocol *(LifeTechonologies, Milan, Italy)*. In each transfection reaction, a plasmid encoding for the EGFP (Enhanced Green Fluorescent Protein) was used to confirm the successful transfection procedure. Total cDNA in the transfection mixture was kept constant at 4 μg for electrophysiological experiments and 6 μg for Western blotting experiments.

5.4 Patch-clamp recordings

For electrophysiological experiments, CHO or HEK-293 cells were seeded on glass coverslips, previously heat sterilized and pre-coated with poly-L-lysine, in 40 mm dishes. The day after, cells were transiently transfected with 4 μg of total cDNA (3.6 μg of plasmids coding for KCNT1 or KCNT2 channels + 0.4 μg of EGFP) and macroscopic currents were recorded after 24 h at room temperature (22°-24° C) by using the patch-clamp technique in the whole-cell configuration. During patch-clamp recordings the cells were perfused with an extracellular solution containing (in mM): 138 NaCl, 5.4 KCl, 2 $CaCl_2$, 1 $MgCl_2$, 10 glucose, and 10 HEPES, pH 7.4 (adjusted with NaOH). The pipette used for wild-type or mutant KCNT1 channel recordings were filled with an intracellular solution containing (in mM): 130 KCl, 10 NaCl, 10 HEPES, 5 EGTA, 5 Mg-ATP, pH 7.4 (adjusted with HCl). When NaCl was omitted from the pipette solution, KCl concentration was increased accordingly.

The same intracellular solution was used to record wild-type or mutant KCNT2 channel subunits, without addition of ATP since KCNT2 elicited currents are inhibited by ATP [Bhattacharjee et al., 2013].

The data were acquired and analyzed using a commercially available amplifier *(Axopatch 200B, Molecular Devices, Union City, CA, USA)* and pCLAMP10 software *(Axon Instruments)*. Current densities were expressed in picoamperes per picofarad, (pA/pF) and calculated as peak K^+ currents (pA) at all tested membrane potentials divided by cell capacitance (C).

To obtain conductance/voltage curves, cells expressing wild-type or mutant KCNT1 or KCNT2 channels were held at -80 mV, depolarized from -120/-90 mV to +60 mV in 10 mV increments, followed by an isopotential pulse at -80 mV. Currents values were measured, normalized and expressed as a function of the preceding voltage. The data obtained were fit to a *Boltzman* distribution of the following form:

$$y=max/[1 + exp\ (V_{1/2} - V)/k]$$

where "max" is the maximal currents, "V" is the test potential, "$V_{1/2}$" indicate the half-

activation potential, and “k” the slope factor.

Bepridil and quinidine *(Sigma Aldrich, Milan, Italy)* were dissolved in DMSO and chloroform, respectively (final vehicle concentration ≤ 0.05%); tetraethylammonium (TEA) was dissolved in water. In each experiment, the same volume of vehicle used to dissolve each drug to be tested was added to the control solution. In each experiment, the same volume of solvent used to dissolve each drug to be tested was added to the control solution. Drugs were perfused using a fast solution exchange system, and each cell was exposed to only one drug concentration to avoid cumulative block.

5.5 Plasma membrane protein biotinylation and Western Blotting

In order to carry out biotinylation and Western-blotting experiments, CHO cells were seeded on 60 mm Petri dishes (250.000 cells for Petri) and 24 h later transiently transfected with 6 μg of total cDNA (5 μg of wild-type or mutant pCMV6-KCNT1 + 1 μg EGFP). One day after transfection, for biotinylation experiments CHO cells were treated for 30’ at room temperature (RT) with Sulfo-NHS-LC-Biotin *(Pierce, Erembodegem-Aalst, Belgium)*, a cell membrane impermeable reagent, which therefore labels only proteins at plasma membrane. Cells were washed three times with PBS (Phosphate Buffer Saline) added with 100 mM glycine in order to remove the excess of biotin. For biotinylation experiments cells were then lysed in CMF-buffer containing (in mM): 120 NaCl, 50 KCl, 50 NaF, 20 Tris-HCl pH 7.5, 10 EDTA, 2% Triton, 2 DTT, and 1X protease inhibitors *(Roche, Milan, Italy),* while for Western-blotting experiments cells were lysed in B-buffer containing in: 150 mM NaCl, 10 mM Tris-HCl pH 7.4, 1 mM EDTA, 1% SDS and 1X protease inhibitors *(Roche, Milan, Italy)*. An equal amount of cell lysates was reacted with ImmunoPure immobilized streptavidin beads *(Pierce)* for 30’ at 4°C to allow the binding of biotin to the surface of the magnetic beads. The beads (bound to the plasma membrane proteins) were separated and collected using a magnetic support, while the supernatant was used as total lysates (Figure 12).

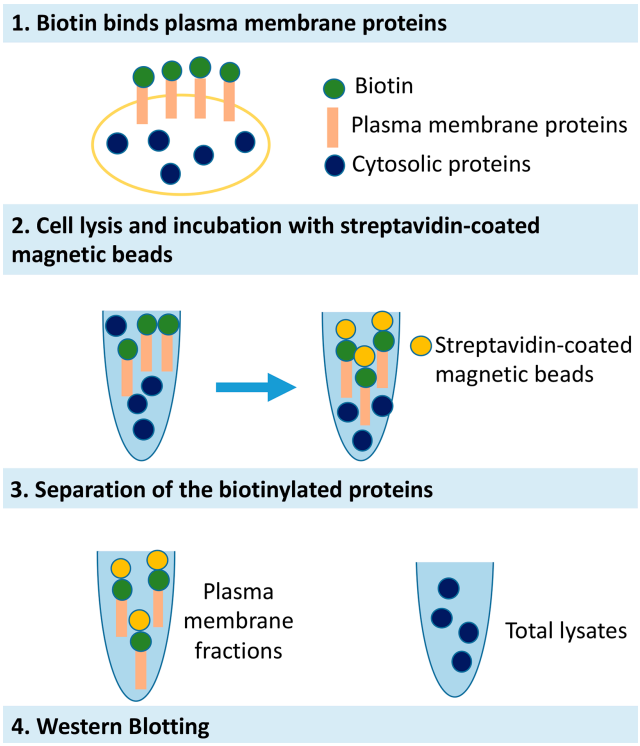

Figure 12 Schematic representation of the biotinylation procedure.

After the biotinylation procedure, the total volume of plasma membrane proteins and an equal amount of total lysates among different samples were separated electrophoretically at RT on 7% SDS-PAGE gels in running buffer (containing 25 mM Tris, 192 mM glycine, 0.1% SDS) until the complete separation of the protein marker loaded in parallel *(Biorad, Milan, Italy)*. Proteins were then transferred onto polyvinylidene fluoride membranes *(PVDF, Biorad, Milan, Italy)* in transfer buffer containg 25 mM Tris, 192 mM glycine, 20% methanol). PVDF membranes were than incubated with 5% milk in the blocking solution (5% milk dissolved in PBS-Tween buffer) to block unspecific binding sites on the membrane for 1h at RT; blots were then incubated with a mouse monoclonal anti-DDK (clone 4C5, dilution 1:1000 in blocking solution; *Origene, Rockville, MD, USA*), mouse polyclonal KCNT1 (dilution 1:2000 in blocking solution; *Ab YOM-655 Primm, Milan, Italy*), mouse monoclonal tGFP (dilution 1:1000 in blocking solution; *Origene, Rockville, MD, USA*) or anti-tubulin (dilution 1:5000 in blocking solution, *Sigma*) antibodies for 16 h at 4°C. After PVDF membrane washing (lasting 30' with PBS-Tween), blots were incubated with anti-mouse secondary antibodies (dilution 1:5000 in blocking

solution, *GE Healthcare, UK*) for 1 h at RT. The secondary antibodies are coniugated with horseradish peroxidase enzyme (HRP), which allows the emission of light in presence of an enhanced chemiluminescence solutions (ECL, *Promega, Madison, WI, USA*). Data acquisition were made by using ImageLab software (*version 4.1; Biorad, Milan, Italy*).

5.6 Molecular modelling

A state-dependent homology model of human KCNT2 was generated starting from the closed (PDB 5U76) and the open (PDB 5U70) configurations of chicken KCNT1 [Hite et al., 2017]. In particular, the H185-T191 loop in the S_4-S_5 linker, whose cryo-EM density was missing in the PDB 5U76 entry, was refined (together with all side chains within 7.5 A°) using the extended sampling protocol of the Prime program [Jacobson et al., 2004].

5.7 Statistics

Data were expressed as the mean ±SEM. Statistically significant differences between the data were evaluated with the Student's *t* test, with the threshold set at $p<0.05$.

6. RESULTS

6.1 Clinical features of patients affected by Epileptic Encephalopathy carrying KCNT1 or KCNT2 mutations

In collaboration with groups of many neurologists, *de novo* mutations in KCNT1 or KCNT2 genes, described in the present Thesis, have been identified in patients affected by severe EE. Clinical features of these patients are summarized in the following table:

Mutation	Sex/ age of seizure onset	Clinical features of patients recruited in the present work	Reference
KCNT1 **c.862 G>A;** **p. G288S** ***(de novo variant)***	Male; 2 months of age	Seizure onset characterized by an episode of sudden crying, psychomotor arrest of short duration followed by prolonged lethargy. Seizures characterized by deviation of the head to the right during sleep, followed quickly by heads and eyes turning to the left, together with tonic contraction of the left arm followed by recurring rhythmic jerks	[Ishii et al., 2013] [Rizzo et al., 2016]
KCNT1 **c.1546 A>G;** **p. M516V** ***(de novo variant)***	Male, second day of life	Seizure activity characterized by apnoea and cyanosis. Focal motor seizures with clonic movements. EEGs recorded multifocal paroxysmal activity with shifting areas of ictal onset (migrating spikes) between hemispheres or overlapping seizures with different areas of ictal onset in different hemispheres	[Rizzo et al., 2016
KCNT1 **c.2677G>A;** **p. E893K** ***(de novo variant)***	Male child, 5 hours of life	EEG showed interhemispheric asynchrony, right central and left temporal slow waves and sharp spikes and waves. Seizures's frequency gradually increased up to 30 episodes per day, characterized by head and gaze deviation (right>left), winking, oral automatisms, sometimes associated with asymmetric upper limb flexor hypertonia (right>left). At four months of age he developed epileptic spasms with hypsarithmic pattern. At 9 months of age, he presented clinical and EEG characteristics of malignant migrating partial seizures of infancy (MMPSI).	newly-identified

Mutation	Sex/ age of seizure onset	Clinical features of patients recruited in the present work	Reference
KCNT1 **c.2849 G>A;** **p. R950Q** ***(de novo variant)***	Male, neonatal onset	Apneas and cyanosis, sometimes associated with pedaling movements and motor agitation. Epilepsy relapsing at the age of two months with focal myoclonus and focal tonic-clonic seizures at the lower limbs related to a EEG central ictal activity, with progressively increasing seizure finally turning in a month into a classical Malignant Migrating Partial Seizure (MMPSI) phenotype.	[Moller et al., 2015]
KCNT2 **c.1451 G>A;** **p. C484Y** ***(inherited variant)***	ND	Nocturnal Frontal Lobe Epilepsy (NFLE)	newly-identified
KCNT2 **c.569 G>A;** **p. R190H** ***(de novo variant)***	Female, 8 months	Clusters of symmetric epileptic spasms and developmental arrest. Semiology evolving from West toward Lennox-Gastaut syndrome.	newly-identified
KCNT2 **c.569 G>C;** **p. R190P** ***(de novo variant)***	Female, first day of life	Abnormal activity in the right temporal region. Grand mal convulsion at 6 months. She was also lax and hypotonic. Speech was delayed. She has severe learning disability. She also self-harms with chewing, poking orifices and scratching.	[DDDS, Nature 2017]

Table 5 KCNT1 and KCNT2 mutations found in patients affected by Epileptic Encephalopathy and studied in the present doctoral thesis.

6.2 Identification of G288S and M516V *de novo* KCNT1 mutations in patients affected by Malignant Migrating Partial Seizures (MMPSI)

Genetic studies performed in collaboration with Prof. A. Weisz (University of Salerno) by using Whole exome sequencing (WES) technique allowed the identification of a new heterozygous missense mutation c.1546 A>G (p. M516V) in proband 1, but not in his healthy parents. The M516 residue is located in the RCK1 (Regulator of Conductance for K^+) domain of the C-terminal region and is highly evolutionarily conserved among species. By contrast, proband 2 carried the already reported KCNT1 mutation c.862G>A (p. G288S) [Ishii et al., 2013] that affects another highly conserved amino acid residue located in the S_5 segment of the protein (Figure 13).

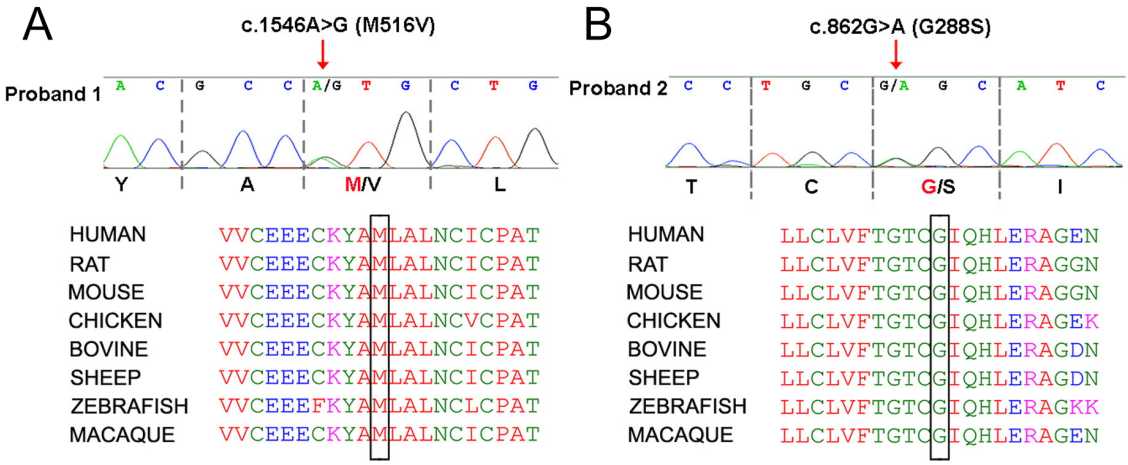

Figure 13 Identification of the M516V and G288S heterozygous mutations found in two patients affected by MMPSI. (A,B) Upper panel: electropherograms obtained from Sanger sequencing of Proband 1 and Proband 2. Lower panel: partial alignment of KCNT1 orthologous peptide sequence from different species. Black boxes indicate the aminoacids influenced by nucleotide mutations

6.3 Functional characterization of homomeric wild-type and mutant G288S and M516V channels

To investigate the functional consequences of G288S and M516V mutations, electrophysiological experiments were performed in CHO cells transiently transfected with plasmids encoding wild-type or mutant KCNT1 subunits. The measurement of currents elicited by wild-type or mutant channels were performed in CHO cells, which do not express these channels endogeneously: indeed in non-transfected CHO cells, after the application of a classical voltage protocol for K^+ currents recordings, no current

was measured above background levels (maximal current density at +60 mV was 1.4 ± 0.6 pA/pF n=5; Fig. 14 A,B). By contrast, CHO cells transfected with wild-type KCNT1 cDNA elicited robust, outwardly-rectifying currents in response to depolarizing voltage pulses from -90 mV to +60 mV. Current density in KCNT1-transfected CHO cells was 112.2±15.7 pA/pF (+60 mV; n=14; Fig. 14 A,B). The application of tetraethylammonium (TEA, 10 mM) reversibly inhibited KCNT1 currents by 47±4% (+40 mV; n=5). KCNT1 currents display complex activation kinetics, with an instantaneous, time-independent component (I_{inst}), followed by a slower, time-dependent one ($I_{steady\text{-}state} - I_{inst}$). At +60 mV, the ratio between currents measured at the beginning (I_{inst}) and at the end ($I_{steady\text{-}state}$) was 0.28±0.01; (n=30). Electrophysiological experiments in CHO cells transiently expressing KCNT1 channels carrying the G288S or the M516V mutations revealed that all mutant channels also generated outwardly-rectifying currents. When compared to wild-type KCNT1 channels, current densities elicited by G288S and M516V mutant channels at +60 mV, were significantly larger, being 269.8±15.3 pA/pF and 170.3±17.0 pA/pF, respectively (n=14-19; $p<0.05$ vs KCNT1; Fig. 14 A, B). No mutation-induced changes in channel selectivity for K^+ ions were observed: in fact, the current reversal potentials estimated from tail current analysis were -68.4±1.2 mV (n=11), - 68.7±0.9 mV (n=13) and -68.9±1.3 mV (n=17) for wild-type KCNT1, KCNT1-G288S and KCNT1-M516V channels, respectively. These values are similar to those reported in the literature for SLO2.2 currents expressed in *Xenopus laevis* oocytes and recorded under similar ionic conditions [Santi et al., 2006]. In KCNT1-G288S and KCNT1-M516V mutant channels, the $I_{inst}/I_{steady\text{-}state}$ were increased when compared to wild-type KCNT1 channels (0.81±0.04 and 0.70±0.03, respectively; n=11-18; $p<0.05$). Moreover, both mutations were able to induce a shift of the G/V curves in the hyperpolarizing direction. Boltzmann analysis of the G/V curves form KCNT1, KCNT1-G288S and KCNT1-M516V mutant channels revealed that the activation midpoints ($V_{1/2}$) were, respectively, 17.5±2.1 mV, -10.5±1.6 and -16.8±1.7, whereas the slopes (ks) were, respectively, 23.9±1.0, 23.0±1.1 and 21.1±1.2 mV/e-fold. Collectively, these results indicate that KCNT1-G288S and KCNT1-M516V mutations induce a strong gain-of-function effect on KCNT1 channels.

In order to study a possible mutation-induced altered sensitivity to regulation by

intracellular cations, patch-clamp recordings were performed in CHO cells transiently expressing wild-type or mutant channels in the presence (10 mM $[Na^+]_i$) or in the absence of $[Na^+]_i$. When NaCl was omitted from the pipette solution, wild-type KCNT1 currents were decreased by a factor of ~ 7, whereas those recorded from KCNT1-M516V or KCNT1-G288S mutant channels were about ~ 2.2 times smaller than those recorded with 10 mM NaCl in the pipette solution (Fig. 14 C). Current density recorded at +60 mV with 10 mM Na^+ or 0 mM Na^+ in the pipette solution were: 109.6±7.7 pA/pF and 16.1±2.9 pA/pF for KCNT1, 260.8±11.2 pA/pF and 111.9±14.8 pA/pF for KCNT1-G288S and 154.6±11.5 pA/pF and 77.2±12.5 pA/pF for KCNT1-M516V. During the entire time of recordings, current density carried by ion channels regulated by intracellular factors, as in the case of KCNT1 currents, may change as a function of time; this may occur because intracellular dialysis of the pipette solution might significantly change the intracellular content of ions like Na^+ and Cl^-, which modulate KCNT1 channel function. Thus, there was a possibility that the differences in current densities observed between wild-type and mutant KCNT1 channels might have been due to the fact that the measurements were carried out at different time points after establishing the whole-cell configuration. Therefore, currents elicited by wild-type or mutant KCNT1 subunits were measured as a function of the time (from 1 to 5 minutes) after the whole-cell access at 0 mV. As demonstrated in Figure 14 D, current amplitudes and kinetic properties of wild-type or mutant subunits were stable during the entire recording period, therefore suggesting that the mutant-induced increase in KCNT1 maximal currents was real and not due to an experimental artifact.

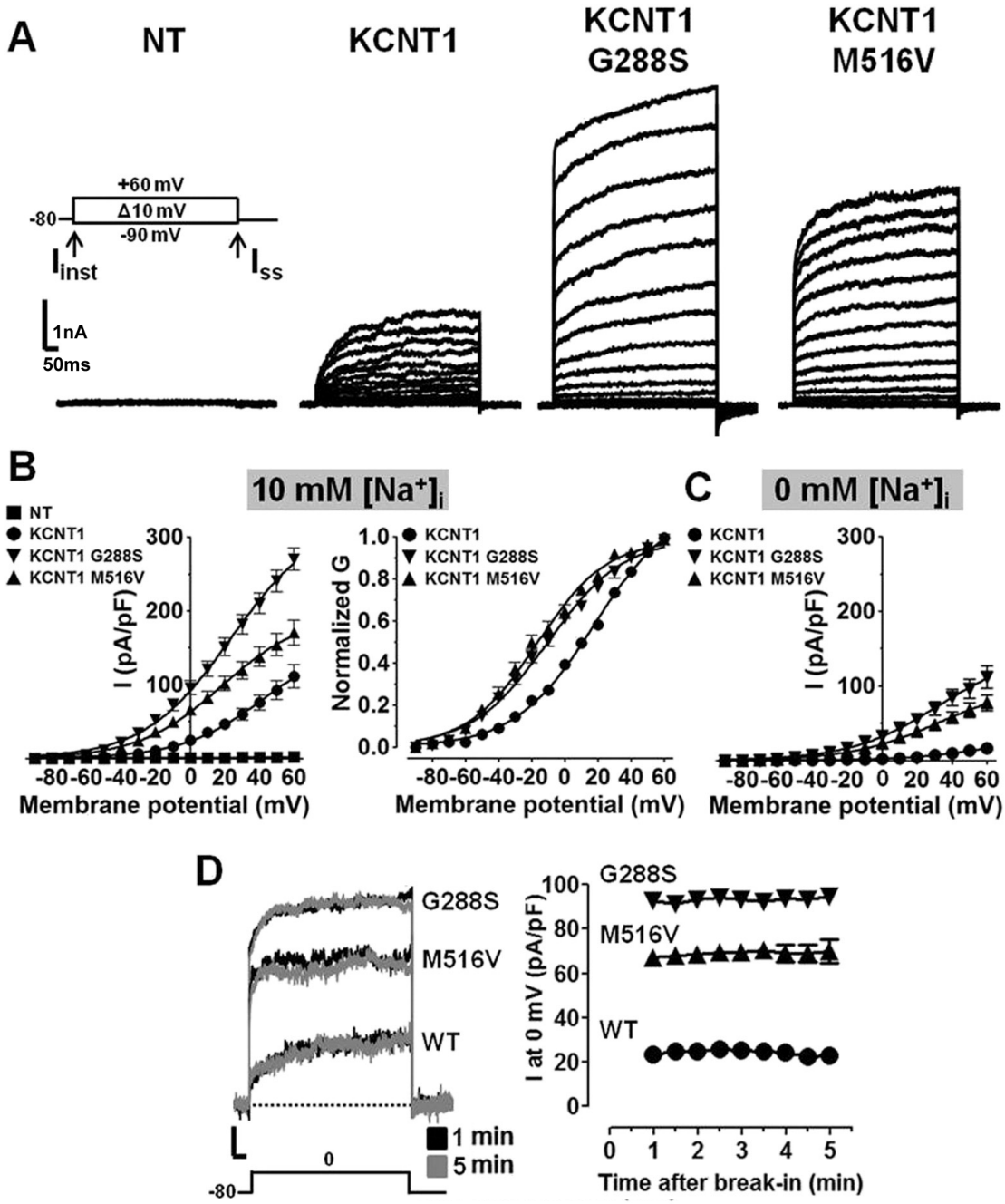

Figure 14 Functional characterization of wild-type and mutant KCNT1 channels. (A) Current traces from CHO cells untransfected (NT) or transfected with expression vectors encoding wild-type or G288S, M516V, mutant channels, as indicated in response to the voltage protocol shown above traces from NT cells. The arrows on the voltage protocol indicate the time chosen for current analysis (I_{inst}= instantaneously-activated currents; I_{ss}= current measured at the steady-state level). (B) Current density (left) and normalized conductance (right) of wild-type or mutant KCNT1 channels, as indicated, recorded with 10 mM NaCl in the pipette (10 mM Na^+). Each point is the mean ± SEM of 5 (NT), 14 (KCNT1), 15 (KCNT1 G288S) or 19 (KCNT1 M516V) determinations, performed in at least three different transfections. (C) Current density of wild-type and mutant KCNT1 channels, recorded without NaCl in the pipette solution (0 mM Na^+). Each point is the mean ± SEM of 11 (KCNT1), 20 (KCNT1 G288S) or 12 (KCNT1 M516V) determinations, performed in at least three different transfections. (D) On the left, representative current traces recorded from wild-type and mutant channels at different times points (1 min, black traces; 5 min gray traces) after whole-cell access at 0 mV. The right panel shows average values of the entire time-course (n=4-7).

6.4 Biochemical assays of total and plasma membrane expression of wild-type and mutant KCNT1 subunits

To evaluate whether the strong gain-of-function effects of KCNT1-G288S and KCNT1-M516V mutant subunits were due to an alteration in total or plasma membrane protein expression levels, western-blotting experiments were performed on total lysates or biotinylated plasma membrane fractions obtained from CHO cells transiently expressing myc-DDK tagged wild-type and mutant KCNT1 subunits (Figure 15). Western-blotting experiments of total protein lysates from CHO cells transfected with wild-type or mutant subunits revealed the expression of a specific band of ~ 130 kDa, a value consistent with the predicted molecular mass of a KCNT1 subunit. Densitometric analysis revealed that the intensity of this band was identical in lysates from KCNT1 and KCNT1 G288S-transfected cells, whereas it was lower in KCNT1 M516V-transfected cells. The $OD_{KCNT1\text{-}TOT}/OD_{TUB}$ ratios were 1.38±0.21; 1.16±0.20 and 0.64±0.14 respectively in the three groups (n=7; $p<0.05$). Similar results were obtained in western-blotting experiments performed in biotinylated plasma membrane fractions. In fact, the intensity of the band corresponding to KCNT1-G288S was similar to that of wild-type KCNT1 ($OD_{KCNT1\text{-}BIOT}/OD_{TUB}$ ratios were 0.87±0.11 and 0.76±0.12, respectively), wheras lower values were measured in KCNT1 M516V-expressing cells (the $OD_{KCNT1\text{-}BIOT}/OD_{TUB}$ was 0.34±0.14).

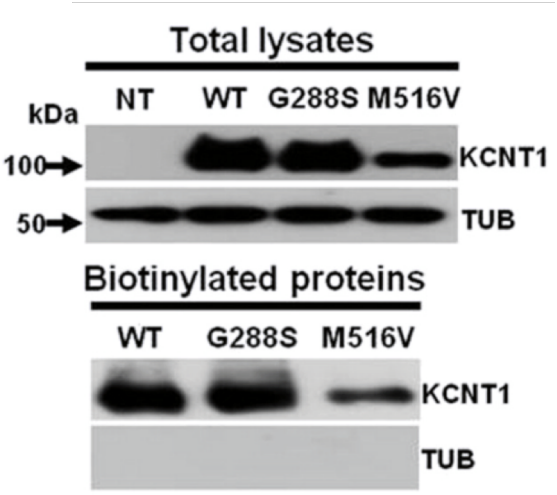

Figure 15 Biochemical characterization of wild-type or mutant KCNT1 channels. Representative images of western-blotting experiments performed on total lysates (upper panels) or plasma membrane-enriched fraction (lower panels) obtained from CHO cells untransfected (NT) or expressing wild-type or mutant subunits, as indicated. In each panel, the higher blots were probed with anti-DDK antibodies to reveal the KCNT1 channels (130 kDa), while the lower panels were probed with anti-α-tubulin (50 kDa), to check for equal protein loading and to confirm that the biotin did not leaks into the cell and labels intracellular proteins. Numbers on the left correspond to the molecular masses of the protein marker.

These results suggest that the M516V, but not the G288S mutation, reduced subunit abundance in both total lysates and plasma membrane fractions: this indicates the absence of a correlation between M516V-induced KCNT1 gain-of-function and protein abundance, as also reported for other mutations [Kim et al., 2014]. In addition, lack of a specific mutation-induced trafficking defect in KCNT1 M516V subunits is supported by the identical absolute ratio between plasma membrane and total protein in cells expressing KCNT1, KCNT1 G288S or KCNT1 M516V: the $OD_{KCNT1\text{-}BIOT}/OD_{KCNT1\text{-}TOT}$ ratios were 1.29±0.16, 1.87±0.70 and 2.06±0.74 respectively (n=6-7; $p<0.05$).

Collectively, these results indicate that the increased current density recorded in CHO cells expressing KCNT1 mutant subunits herein investigated, cannot be ascribed to an enhanced plasma membrane localization or expression.

6.5 Functional characterization of wild-type and mutant KCNT1 in heteromeric configuration

As mentioned above, genetic analysis of the two probands revealed that both *de novo* mutations herein investigated were found heterozygously in the KCNT1 gene. For this reason, to mimic the genetic condition of these MMPSI-affected patients, wild-type and mutant KCNT1 cDNAs were co-transfected in CHO cells at a 0.5:0.5 ratios. As shown in Figure 16, currents elicited from KCNT1/KCNT1 G288S and KCNT1/KCNT1 M516V heteromers were still larger than those from KCNT1 homomers ($p<0.05$), but reduced compared to those recorded in cells expressing corresponding homomeric channels (Figure 14 A).

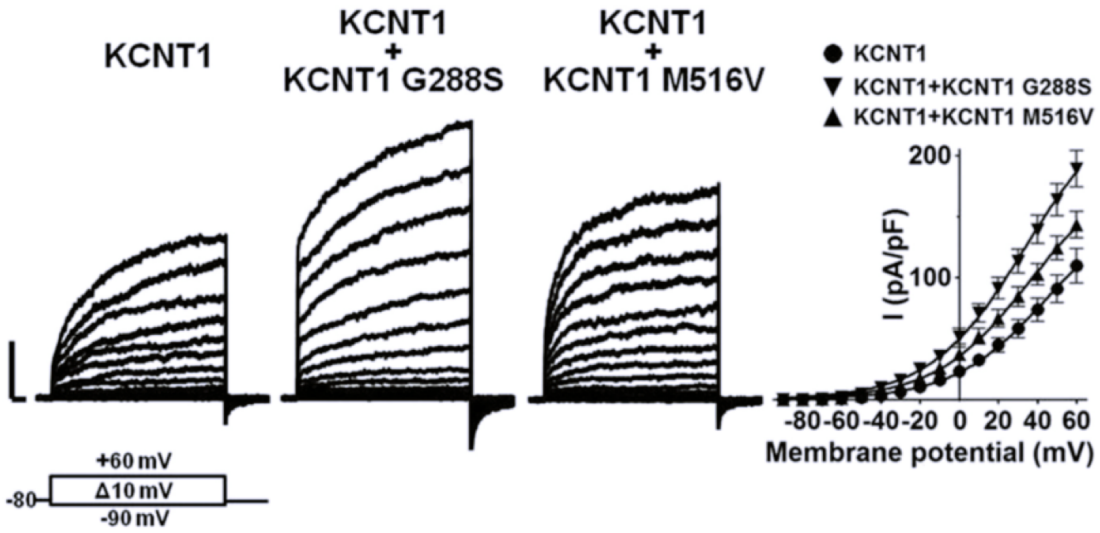

Figure 16 Macroscopic currents measured in cells expressing KCNT1 heteromeric channels formed by wild-type and mutant KCNT1 channels. Representative current traces (left three panels) and pooled current densities from CHO cells expressing KCNT1 homomers or KCNT1+KCNT1-G288S or KCNT1+KCNT1-M516V heteromers, as indicated (current scale: 1nA; time scale: 50 ms). In the right panel, each data point is the mean ± SEM of 13-16 determinations, each form a single cell, recorded in at least three different transfections.

Furthermore, $I_{inst}/I_{steady\text{-}state}$ ratios at +60 mV were 0.51±0.03, 0.41±0.03 and 0.28±0.01 respectively ($p<0.05$), for KCNT1/KCNT1 G288S, KCNT1/KCNT1 M516V and KCNT1 channels ($p<0.05$ versus KCNT1). The fact that current density values and $I_{inst}/I_{steady\text{-}state}$ ratios in cells expressing heteromeric wild-type/mutant channels were smaller than those recorded in cells expressing mutant homomers allows to hypothesize that the mutation-induced gating changes depends on the number of mutant subunits

incorporated, being larger in homomeric configuration (with 4 mutant subunits) than in heteromeric (likely to carry an average of 2 mutant subunits) channels. However, these results could also be explained by the fact that only homomeric channels (wild-type or mutant) are present at the plasma membrane level, therefore excluding the possibility that heteromeric channels can be obtained: as mutations herein investigated do not fall in the KCNT1 domain presumably responsible for intersubunit interactions, this latter hypothesis should be excluded, although this issue requires further investigation.

6.6 Pharmacological characterization of G288S and M516V mutant channels

As reported in the *Introduction* section, bepridil and quinidine are two well-known KCNT1 current blockers. In order to characterize the pharmacological sensitivity of wild-type and mutant KCNT1 channels to these compounds, we tested the effects of bepridil at the concentrations of 0.1-10 μM (Figure 17 A) and of quinidine at the concentrations of 10-1000 μM (Figure 17 B). Both drugs produced a concentration-dependent decrease in KCNT1 outward currents with IC_{50s} at +60 mV of 1.1 ± 0.1 μM and 82.1±14.3 μM, respectively. Both bepridil and quinidine inhibited KCNT1 currents over the entire voltage range of activation, although the blocking potency was slightly smaller at less depolarized voltages (at -20 mV, the IC_{50s} for bepridil- and quinidine-induced KCNT1 blockade were 2.8±1.6 μM and 157±20 μM respectively). When compared to KCNT1, bepridil was even more potent in blocking KCNT1-G288S (in fact IC_{50s} was 0.15±0.05 μM; $p<0.05$ versus KCNT1) or KCNT1-M516V (IC_{50s} was 0.3±0.1 μM; $p<0.05$ versus KCNT1) channels. When quinidine was tested on mutant KCNT1 channels, a similar trend was also observed, although differences were less pronounced and failed to reach statistical significance. In fact, quinidine IC_{50s} were 46±12 μM and 67±19 μM for KCNT1-G288S ($p=0.057$ versus KCNT1) and KCNT1-M516V channels ($p= 0.54$ versus KCNT1), respectively. Notably, when bepridil or quinidine were tested up to 0.1 μM and 10 μM respectively, no current inhibition was observed for KCNT1 channels, whereas highly-significant blockade (ranging from 20%-40%) was observed for both KCNT1-G288S and KCNT1-M516V mediated currents within the same drug concentration range ($p<0.05$ for both mutant channels versus wild-type KCNT1).

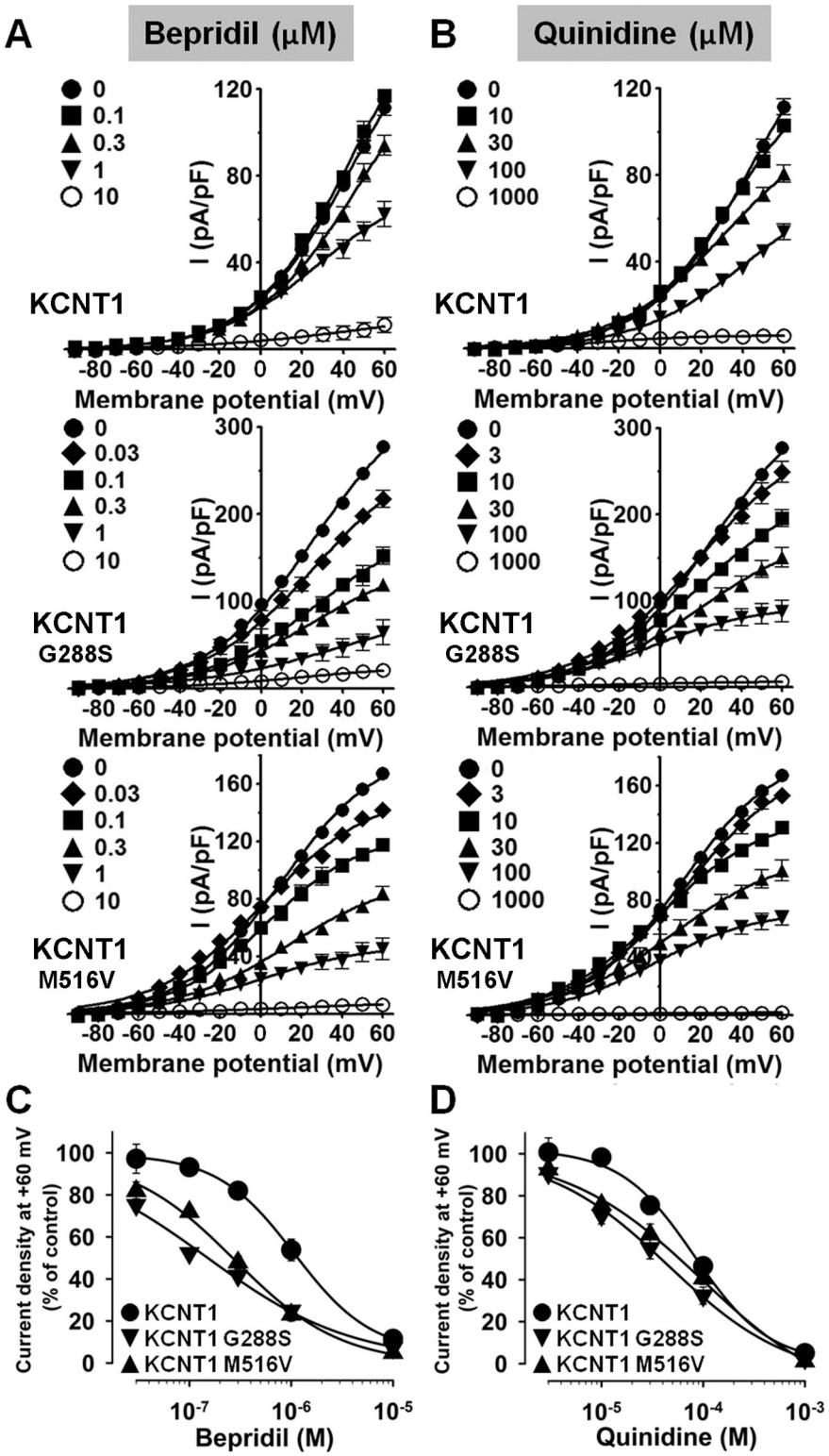

Figure 17 Pharmacological characterization of the current expressed by wild-type or mutant KCNT1 channels. (A-B) Pooled current densities from CHO cells expressing wild-type or mutant KCNT1 channels, as indicated, in control solution or upon exposure to bepridil (A; 10-1000 μM) or quinidine (B; 0.1-10 μM). (C-D) Concentration-dependent inhibition by bepridil (C) or quinidine (D) of wild-type or KCNT1-G288S, KCNT1-M516V mutant channels. Current density after each drug concentration was expressed as % of the control current; normalized data were fitted to the following binding isotherm: $y=max/(1 + x/EC_{50})^n$, where x is the drug concentration and n the Hill coefficient. Each data point is the mean ± SEM of 3-4 (for bepridil) and 3-27 (for quinidine) determinations.

6.7 Biochemical and functional characterization of KCNT1-E893K and KCNT1-R950Q mutant subunits

Prompted by the intriguing results obtained in the studies of KCNT1-G288S and KCNT1-M516V mutations and to deepen knowledge on pathogenic aspects of KCNT1 gene variants in epileptic encephalopathies, we investigated the effects induced by two additional KCNT1 mutations (E893K and R950Q) found in patients (proband 3 and proband 4) affected by MMPSI.

Both E893 and R950 residues are located in the second RCK domain of the channel and are evolutionarily conserved among different species (Figure 18).

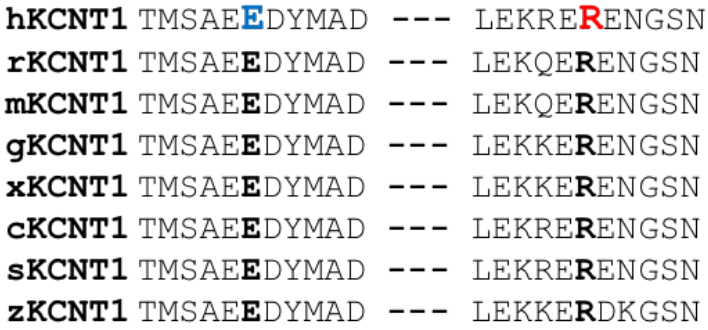

Figure 18 The E893 and R950 residues are evolutionarily conserved among different species. Partial alignment of KCNT1 subunits of different species (h=human, r=rat, m=mouse, g=chicken, x=Xenopus laevis, c=cat, s=sheep, z=zebrafish.

Western-blotting experiments performed in total lysates of CHO cells transiently expressing wild-type or mutant subunits revealed that the presence of E893K and R950Q mutations does not interfere with the expression levels of KCNT1 subunits (Figure 19). In fact, the $OD_{KCNT1\text{-}TOT}/OD_{TUB}$ ratios were: 1.00±0.20, 1.95±0.25 and 2.40±0.55 (n=3; p>0.05) for KCNT1, KCNT1-E893K and KCNT1-R950Q mutant subunits, respectively.

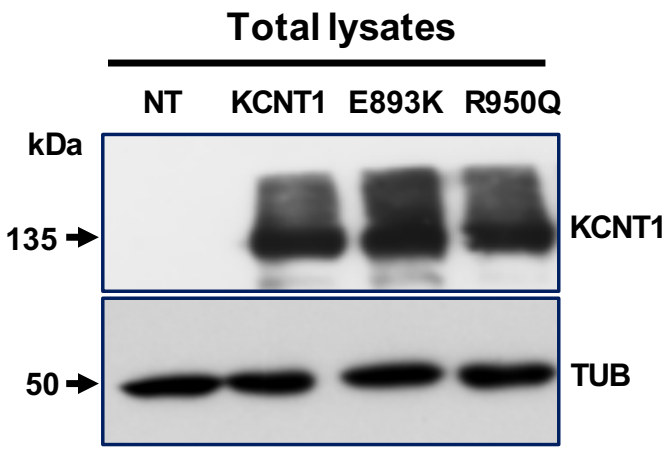

Figure 19 Biochemical characterization of wild-type or mutant KCNT1 channels. Representative image of Western-blotting experiments performed on total lysates obtained from untransfected (NT) CHO or transfected CHO cells expressing KCNT1, KCNT1-E893K or KCNT1-R950Q mutant subunits. The higher blot was probed with anti-KCNT1 antibodies (135 kDa), while the lower panel was probed with anti-γ-tubulin (50 kDa), to check for equal protein loading. Numbers on the left correspond to the molecular masses of the protein marker.

Patch-clamp recordings revealed that current densities expressed by KCNT1-E893K and KCNT1-R950Q mutant channels were significantly larger (Figure 20 A) when compared to KCNT1-transfected cells: in fact, current densities were 229.0±20.3 pA/pF and 231.3±21.1 pA/pF, respectively (n=21; $p<0.05$ versus wild-type KCNT1). Furthermore, in both KCNT1-E893K and KCNT1-R950Q mutant channels, the I_{inst}-$I_{steady\text{-}state}$ ratio was increased when compared to KCNT1, being 0.81±0.03 and 0.44±0.04, respectively (n=13-20; $p<0.05$ versus wild-type KCNT1 channels). The G/V curves for KCNT1 E893K and R950Q were shifted in the hyperpolarizing direction: accordingly, Boltzmann analysis of the G/V curves from KCNT1, KCNT1-E893K and KCNT1-R950Q mutant channels revealed that the activation midpoint ($V_{1/2}$) was, respectively, 17.5±2.1 mV, -39.7±1.3, or -19.4±1.4 mV ($p<0.05$ versus KCNT1), whereas the slopes (*k*s) was, respectively, 23.9±1.0, 17.9±1.2, or 19.6±1.0 mV/e-fold ($p>0.05$ versus KCNT1).

Taken together, these results indicate that also the presence of these mutations leads to strong gain-of-function effects on KCNT1 currents.

In addition, in order to verify if the presence of E893K and R950Q mutations interferes with the Na^+-dependent KCNT1 activation process, additional functional experiments were performed without NaCl in the pipette solution. The results obtained showed that wild-type KCNT1 currents were decreased by a factor of ~5, whereas those from KCNT1-E893K or KCNT1-R950Q channels were about 2- or 4.4-times smaller than those

recorded with 10 mM NaCl in the pipette: in fact, current densities recorded at +60 mV in the presence (10 mM Na^+) or in the absence of Na^+ were 104.1±11.4 or 20.0±2.9 pA/pF, 229.0±20.3 or 101.0±17.6 pA/pF, and 231.3±21.1 or 52.3±10.5 pA/pF for KCNT1, KCNT1-E893K, and KCNT1-R950Q channels, respectively ($p<0.05$ versus wild-type KCNT1 channels (Figure 20 B,C). These results suggest that both KCNT1 mutations, and particularly the E893K variant, significantly alter the Na^+-dependent mechanism of KCNT1 current activation.

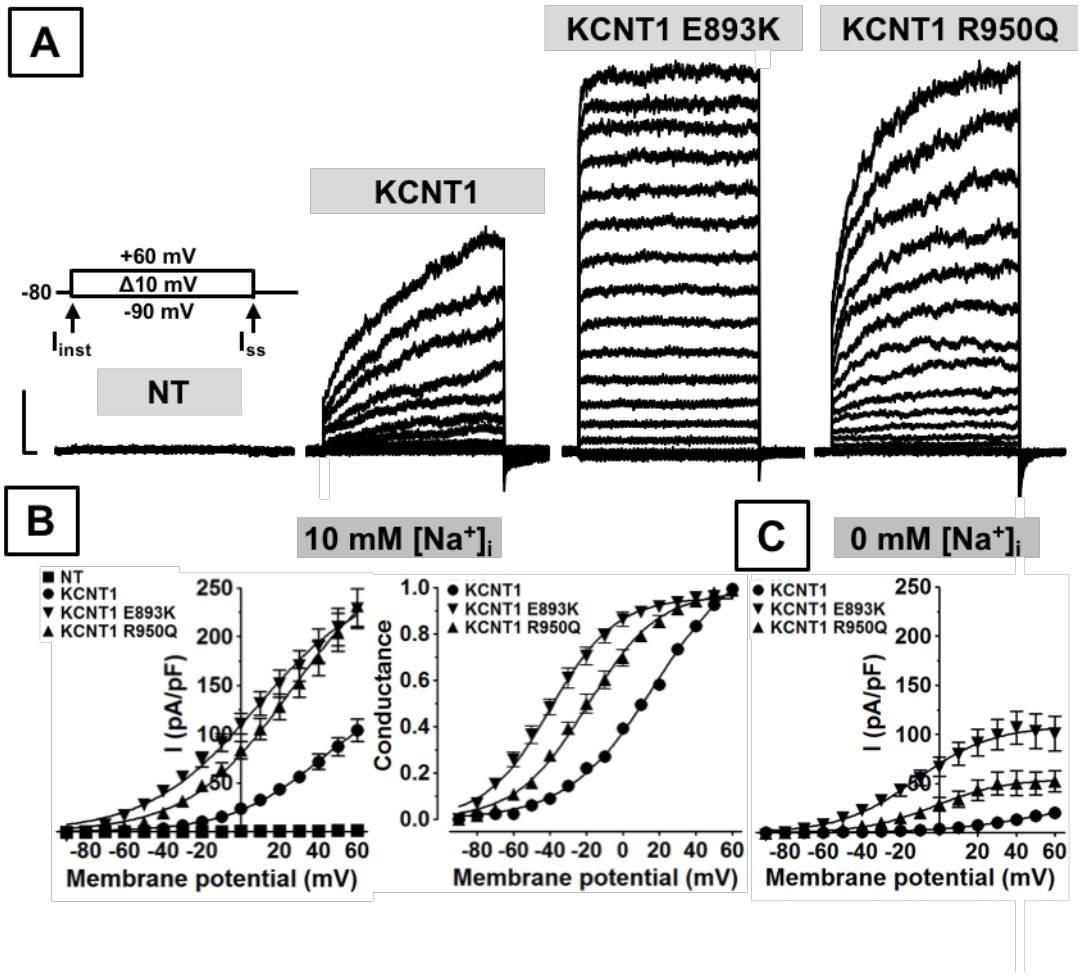

Figure 20 Functional characterization of wild-type or mutant KCNT1 channels. (A) Macroscopic current from CHO cells untransfected (NT) or transfected with expression vectors encoding for wild-type or E893K mutant subunits (current scale: 500 pA; time scale 50 ms). (B) Current density (left) and normalized conductance (right) of wild-type and mutant KCNT1 subunits, as indicated recorded with 10 mM NaCl (10 mM Na^+). Each point is the mean ± SEM of 5 (NT), 29 (KCNT1), 21 (KCNT1-E893K) and 21 (KCNT1-R950Q) determinations, performed in at least three different transfections. (C) Current density of wild-type and mutant KCNT1 channels, recorded without NaCl in the pipette solution (0 mM Na^+). Each point is the mean ± SEM of 29 (KCNT1), 21 (KCNT1-E893K) and 21(KCNT1-R950Q) determinations, performed in at least three different transfections.

6.8 Pharmacological characterization of E893K and R950Q mutant channels by quinidine

In order to verify the possibility to counteract the gain-of-function effects induced by E893K or R950Q mutations, the well-known KCNT1 current blocker quinidine was tested on CHO cells transiently expressing wild-type or mutant subunits. Quinidine was perfused at four different concentrations (1 μM, 10 μM, 100 μM or 1000 μM; Figure 21 A, B, C, D).

The perfusion of quinidine on currents elicited by KCNT1-E893K and KCNT1-R950Q mutant channels induced current inhibition, with higher sensitivity when compared to wild-type KCNT1 channels. In fact, IC_{50}s were: 81.8±0.1 μM, 9.6±2.5 μM and 24.0±5.7 μM (n=19-28; $p<0.05$). In particular, 10 μM quinidine was able to induce a significant blockade of KCNT1-E893K and KCNT1-R950Q currents, without affecting those elicited by wild-type KCNT1 channels.

Collectively these results indicate that quinidine could be useful to counteract the excess of current elicited by mutant channel subunits; in addition, the slightly higher potency of the drug in blocking mutant versus wild-type KCNT1 currents indicates a preferential drug interaction with mutant subunits, possibly due to the open-channel blocking mechanism of quinidine in KCNT1.

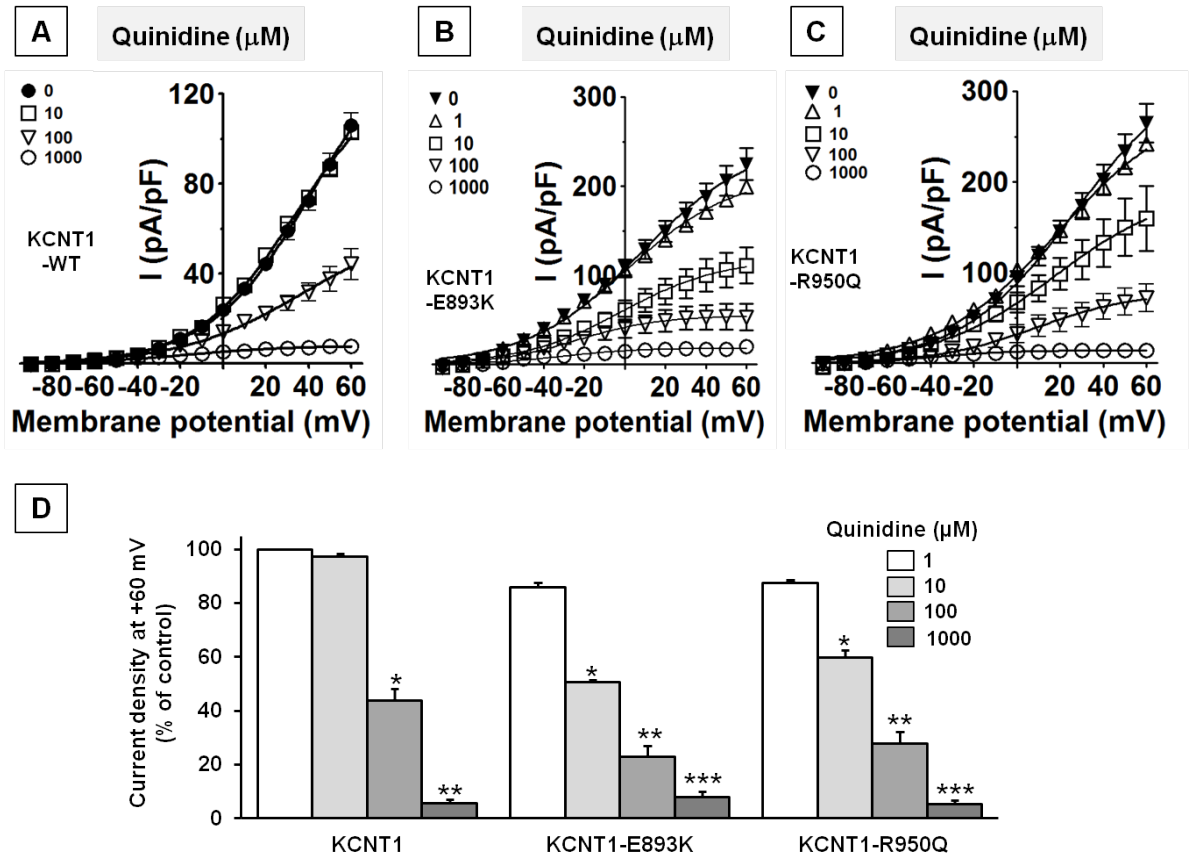

Figure 21 Pharmacological characterization of the currents expressed by wild-type or E893K and R950Q mutant channels. (A,B,C) Pooled current density data from CHO cells expressing wild-type or mutant KCNT1 channels, as indicated, in control solution or upon exposure to quinidine at two different concentrations (100 μM or 1000 μM). (D) Normalized current density at +60 mV from CHO cells expressing wild-type or mutant KCNT1 channels, as indicated, as a function of quinidine concentrations (0. 100 or 1000 μM). For each panel, single or multiple asterisks indicate the values significantly different ($p<0.05$) from those immediately lower quinidine concentration; # indicate values significantly different from those obtained at the same quinidine concentration on wild-type channels.

6.9 Biochemical evidence for KCNT2 channels expression in total lysates of CHO and HEK 293 cells

To assess the functional effects of the KCNT2 mutations, biochemical and functional approaches similar to those applied for KCNT1 were used to study wild-type or mutant KCNT2 channels.

Firstly, channels expression was assessed in two different heterologous expression systems. Western blotting experiments were performed in total lysates from CHO and HEK293 cells transiently expressing wild-type or KCNT2-C484Y mutant channels.

Wild-type and mutant KCNT2 subunits were detected by using anti-turbo GFP antibodies: a single band of ~130 kDa was detected in the lanes corresponding to lysates of HEK293 cells expressing wild-type or mutant channels, while no signals were detected in total lysates of CHO cells expressing wild-type or mutant KCNT2 channels, nor in non-transfected HEK293 or CHO cells. Furthermore, to check for equal protein loading, the same lysates were probed with anti-γ-tubulin antibody (50 kDa, Figure 22). The results obtained indicate that HEK293 cells, but not CHO cells, are efficient *in vitro* heterologous expression system to study the functional properties of wild-type or mutant KCNT2 channels. In addition, the presence of C484Y mutation does not induce an alteration of protein expression levels; in fact, the $OD_{KCNT2\text{-}TOT}/OD_{TUB}$ were 1.00±0.16 and 1.73±0.50 (n=5 p>0.05) for wild-type or mutant KCNT2 subunits, respectively.

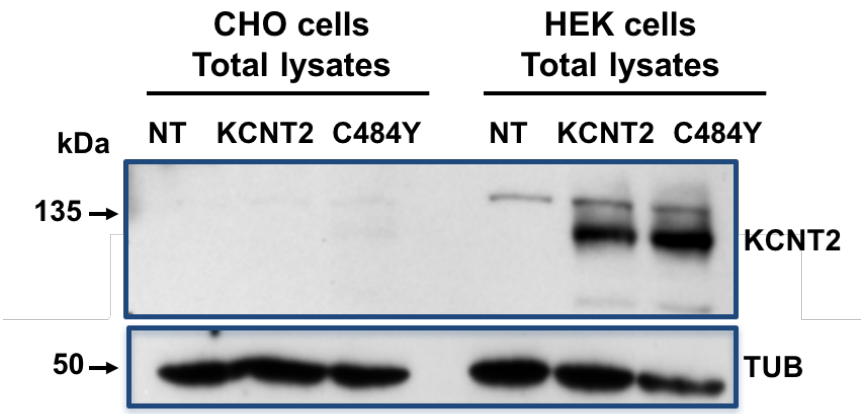

Figure 22 Biochemical characterization of wild-type or mutant KCNT2 channels in two different heterologous expression systems. Representative images of western-blotting experiments on total lysates obtained from untransfected (NT) CHO or HEK293 cells or transfected CHO or HEK293 expressing wild-type or mutant subunits. The higher blots were probed with anti turbo-GFP antibodies to reveal the protein of interest (135 kDa), while the lower panel was probed with anti-γ-tubulin (50 kDa), to check for equal protein loading. Numbers on the left correspond to the molecular masses of the protein marker.

6.10 Functional effects of the C484Y variant on KCNT2 channel function

In order to evaluate whether the C484Y variant found in a family in which the proband was affected with ADNFLE was able to induce functional changes in KCNT2 channels, HEK 293 cells were transiently transfected with plasmids encoding wild-type or mutant KCNT2-C484Y subunits. Patch-clamp recordings in cells expressing wild-type KCNT2 subunits gave rise to outwardly rectifying potassium currents with a threshold potential for activation of -40 mV in response to depolarizing voltage pulses from -120 mV to +60 mV. In this set of experiments, current density in KCNT2-transfected cells was 44.6±2.7 pA/pF; (n=52). KCNT2 currents displayed complex activation kinetics, with an instantaneous, time-independent component (I_{inst}) followed by a slower, time-dependent one ($I_{steady\text{-}state}$-I_{inst}). At +60 mV, the ratio between the currents measured at the beginning (I_{inst}) and at the end ($I_{steady\text{-}state}$-I_{inst}) was 0.49±0.02 (n=52).

Expression of KCNT2 channels carrying the C484Y variant also generated outwardly-rectifying currents; when compared to KCNT2-transfected cells, current densities at +60 mV were not significantly different than those elicited from wild-type KCNT2 channels being 38.7±2.1 pA/pF (n=37) (Figure 23 A, B).

Furthermore, the presence of the KCNT2-C484Y mutation was unable to induce an alteration in the voltage-dependence of activation when compared to wild-type KCNT2 channels. Boltzmann analysis of the G/V curves from KCNT2 and KCNT2-C484Y mutant channels revealed that the activation midpoint ($V_{1/2}$) was -8.7±1.1 mV and -9.1±0.9 mV, respectively ($p>0.05$) whereas the slopes (k_s) were respectively 13.0±0.6 and 11.7±0.5 mV/e-fold for wild-type KCNT2 and KCNT2-C484Y channels ($p>0.05$).

Taken together, these results indicate that the presence of C484Y mutation does not cause detectable changes in KCNT2 channels functional properties when compared to wild-type KCNT2 channels.

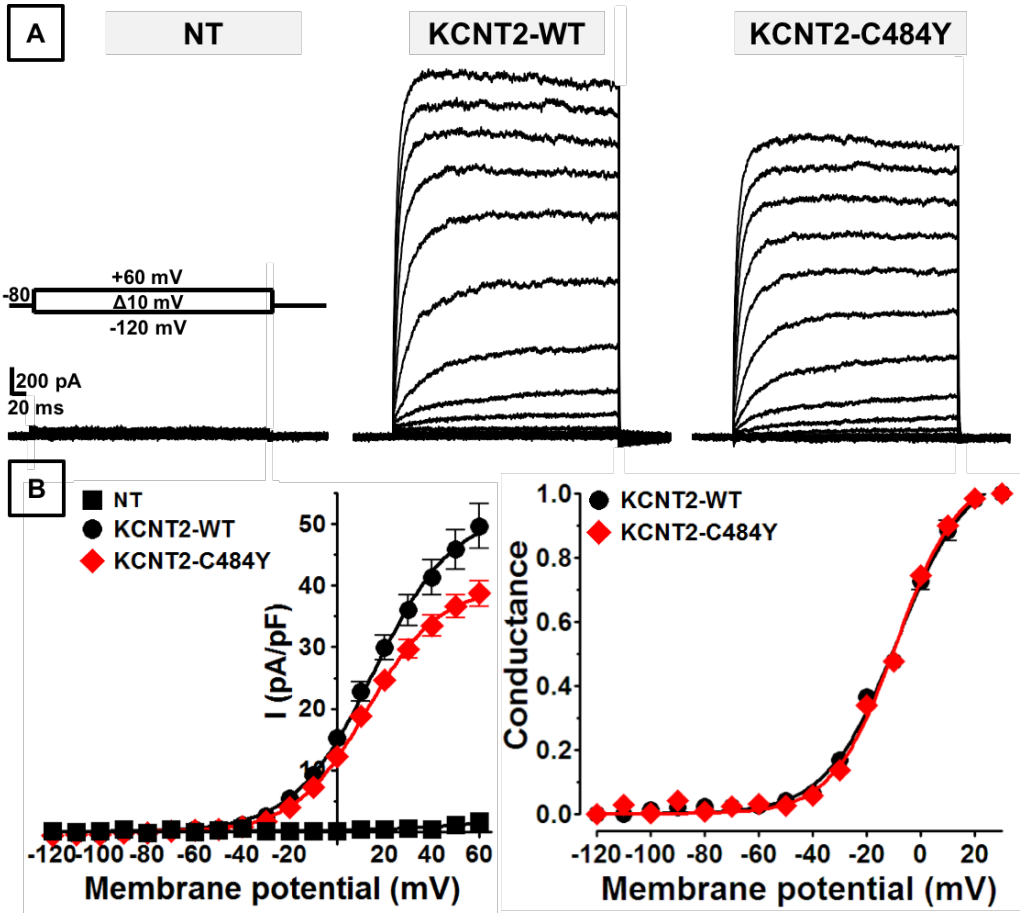

Figure 23 Functional characterization of wild-type and mutant C484Y KCNT2 channels. (A) Current traces from HEK-293 cells untransfected (NT) or transfected with expression vectors encoding wild-type or mutant KCNT2 subunits, as indicated, in response to the voltage protocol. (B) Current density of wild-type and mutant KCNT2 channels. Each point is the mean ± SEM of 2 (NT), 31 (KCNT2) and 37 (KCNT2-C484Y) determinations, performed in at least two different transfections. (C) Normalized conductance of wil-type and mutant C484Y channels, as indicated.

6.11 Biochemical and functional effects of the R190H and R190P mutant subunits

In collaboration with Prof. J. Lemke (Institute of Human Genetics, University of Leipzig Hospital and Clinics) we identified two *de novo* variants in the KCNT2 gene affecting the same residue (R190H and R190P) in two probands with EE. As shown in Figure 24, the R190 residue is located within the S_4-S_5 linker region and is evolutionarily conserved among different species.

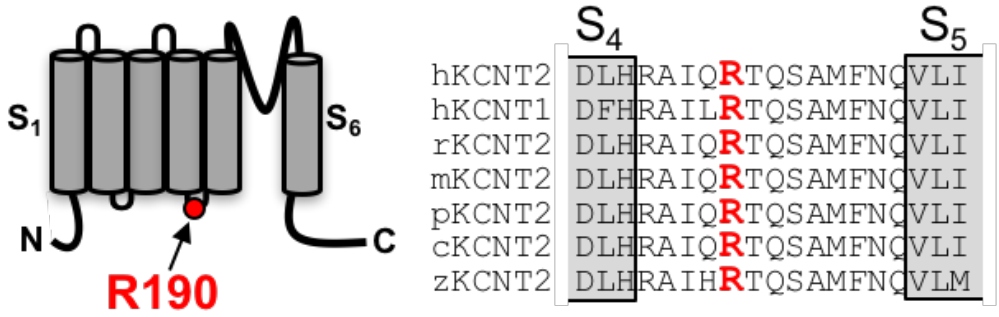

Figure 24 Topological representation of a KCNT2 subunits and partial alignment among orthologous and human KCNT2 proteins. Left, topological representation of a KCNT2 subunits: gray boxes indicate transmembrane segments, while the red circle and arrow indicate the position of the mutated residue found in patients affected by Developmental and Epileptic Encephalopathy. Right, partial alignment of KCNT2 orthologous among different species (h=human; r=rat; m=mouse; p=pig; c=cat; z=zebrafish). The end of the S_4 segment and the beginning of S_5 transmembrane segments, according to Uniprot database, are delimited by gray boxes. The red "R" indicate the R190 residue.

Western-blotting experiments performed in total lysates of HEK-293 cells transiently expressing wild-type or mutant subunits revealed that the presence of R190H mutation does not interfere with the expression levels of KCNT2 subunits, while a significant increase in the expression levels were observed for R190P mutations (Figure 25). In fact, the $OD_{KCNT2\text{-}TOT}/OD_{TUB}$ ratios were: 1.00 ± 0.03 for wild-type KCNT2, 0.49 ± 0.08 for KCNT2-R190H and 1.56 ± 0.14 for KCNT2-R190P mutant subunits ($n=3$; $p<0.05$ versus wild-type KCNT2).

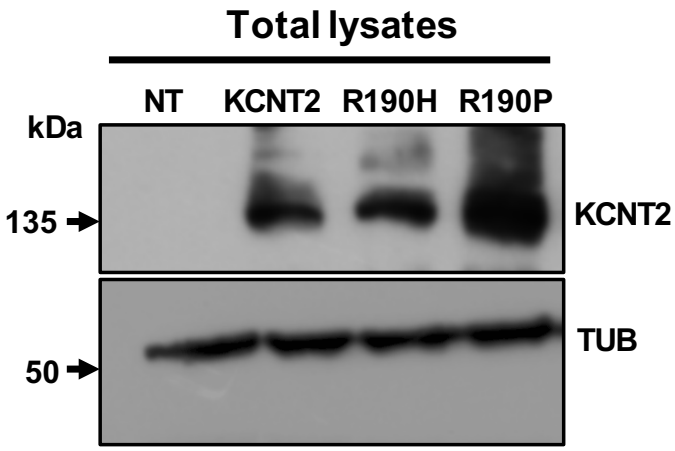

Figure 25 Biochemical characterization of wild-type or mutant KCNT2 channels. Representative image of Western-blotting experiments performed on total lysates obtained from untransfected (NT) HEK-293 or transfected HEK-293 cells expressing KCNT2, KCNT2-R190H or KCNT2-190P mutant subunits. The higher blot was probed with anti-tGFP antibodies in order to reveal the protein of interest (135 kDa), while the lower panel was probed with anti-α tubulin (50 kDa), to check for equal protein loading. Numbers on the left correspond to the molecular masses of the protein marker.

In order to study the functional effects prompted by these mutations on KCNT2 channels, patch-clamp experiments were performed in HEK-293 cells transiently transfected with plasmids encoding wild-type or mutant KCNT2 subunits.

Expression of KCNT2 channels carrying the R190H or the R190P mutations generated outwardly-rectifying currents being significantly larger when compared to wild-type currents (current densities at +60 mV were 147.5±13.6 pA/pF and 398.3±45.5 pA/pF, respectively; n=49-24; $p<0.05$ versus KCNT2; Figure 26).

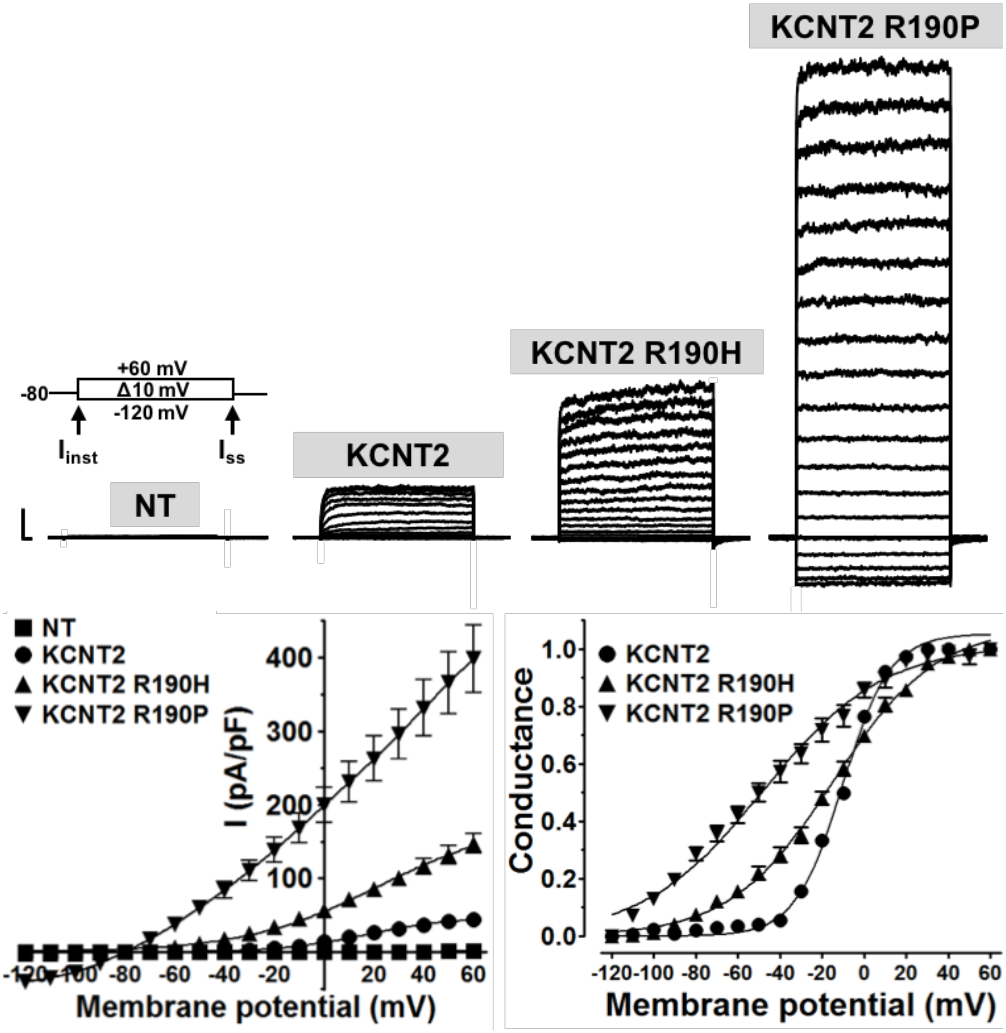

Figure 26 Functional characterization of wild-type or mutant KCNT2 channels. (A) Current traces from untransfected (NT) or transfected HEK-293 cells with plasmids encoding for wild-type or mutant KCNT2 channels, as indicated, in response to the voltage protocol shown above traces from NT cells. The arrows on the voltage protocol indicate the times chosen for current analysis (I_{inst}= instantaneously-activated currents; I_{ss}= current measured at the steady-state level). Current scale: 500 pA; time scale 20 msec. (B,C) Current density (left) and normalized conductance (right) of wild-type and mutant KCNT2 channels. Each data point is the mean ± SEM of 24-52 determinations, each from a single cell, recorded in at least three different transfections.

No mutation-induced changes in channel selectivity for K^+ ions were observed: in fact, the current reversal estimated from tail current analysis were -67.5±0.9 mV (n=34), -63.5±1.3 mV (n=14) and -62.7±1.0 mV (n=12) for KCNT2, KCNT2-R190H and KCNT2-R190P channels respectively. In KCNT2 R190P and R190H mutant channels, the $I_{inst}/I_{steady\text{-}state}$ ratios were significantly increased when compared to KCNT2 (0.77±0.02 and 0.93±0.01, respectively; n=49-24; $p<0.05$). The G/V curves for KCNT2, KCNT2-R190H and KCNT2-R190P were shifted in the hyperpolarizing directions: Boltzmann analysis of the G/V curves from wild-type KCNT2, KCNT2-R190H and KCNT2-R190P mutant channels revealed that the activation midpoints ($V_{1/2}$) were, respectively, -

10.3±0.7 mV, -14.9 ±1.8 mV and -48.0±2.3 mV, ($p<0.05$ versus KCNT2), whereas the slopes (k) were respectively 11.3±0.4, 24.5±1.0 and 28.6±1.6 mV/e fold; ($n=24-52$; $p<0.05$).

Collectively, these results indicate that both R190H and R190P mutations herein identified lead to strong gain-of-function effects on KCNT2 currents.

6.12 Functional characterization of heteromeric channels formed by wild-type or mutant KCNT2 subunits

To reproduce the genetic status of patients herein investigated, who carry only one mutated KCNT2 allele, wild-type and mutant KCNT2 cDNAs were co-transfected in HEK-293 cells at a 0.5:0.5 ratio. As shown in Fig. 27, currents from KCNT2/KCNT2-R190H and KCNT2/KCNT2-R190P heteromers displayed functional properties roughly intermediate between homomeric wild-type and mutant KCNT2 channels: in fact, current densities at +60 mV were 86.1±6.3 pA/pF for KCNT2+KCNT2-R190H ($n=17$; $p<0.05$ versus KCNT2 and KCNT2-R190H) and 250.2±16.2 pA/pF for KCNT2+KCNT2-R190P ($n=15$; $p<0.05$ versus KCNT2 and KCNT2-R190P). Moreover, $I_{inst}/I_{steady\text{-}state}$ ratios at +60 mV were 0.61±0.03 for KCNT2+KCNT2-R190H ($p<0.05$ versus KCNT2 and KCNT2-R190H), and 0.80±0.04 for KCNT2+KCNT2-R190P ($p<0.05$ versus KCNT2 and KCNT2-R190P), respectively.

Boltzmann analysis of the G/V curves from KCNT2+KCNT2-R190H and KCNT2+KCNT2-R190P heteromeric channels, revealed that the activation midpoints ($V_{1/2}$) were -10.1±1.9 mV and -40.4±2.9 mV, respectively ($p<0.05$ versus KCNT2), whereas the slopes (k) were 21.1±1.2 and 27.8±2.0 mV/e-fold for KCNT2+KCNT2-R190H and KCNT2+KCNT2-R190P ($p<0.05$ versus KCNT2).

As observed for KCNT1 mutations, the fact that current density values and $I_{inst}/I_{steady\ state}$ ratios in cells expressing heteromeric wild-type/mutant channels were intermediate between homomeric wild-type and mutant channels allows to hypothesize that the extent of mutation-induced gating changes depends on the number of mutant subunits incorporated, being larger in homomeric (4 mutant subunits) than in heteromeric configuration carrying an average of 2 mutant subunits.

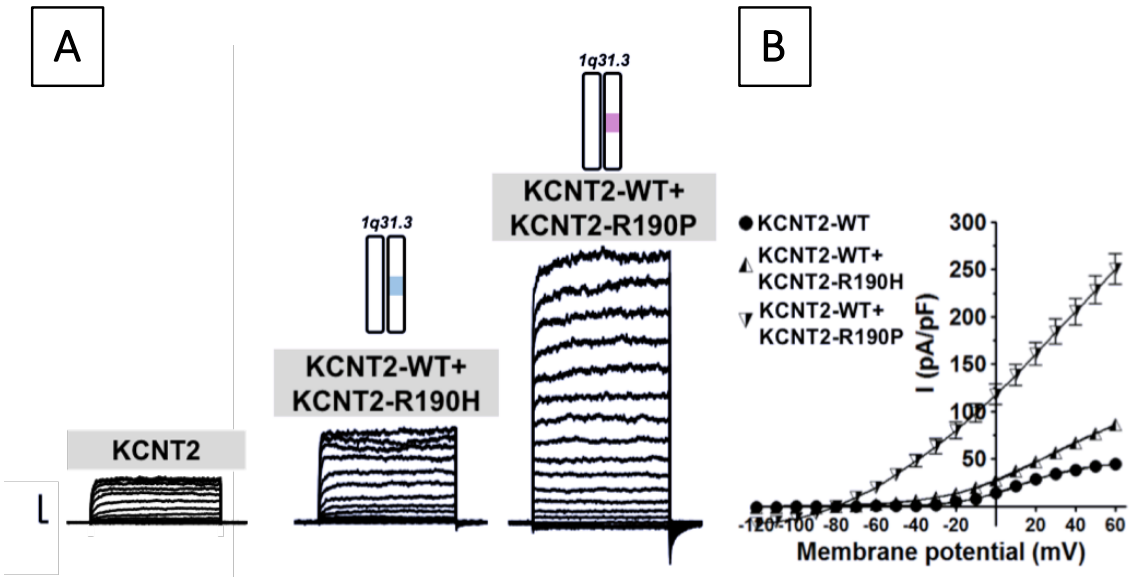

Figure 27 Functional characterization of heteromeric KCNT2 channels. (A) Representative current traces (left three panels) and pooled current densities (right panel) from HEK-293 cells expressing KCNT2 homomers or KCNT2+KCNT2-R190H or KCNT2+KCNT2-R190P heteromers, as indicated (current scale 500 pA, time scale 20 msec). (B) In the right panel, each data point is the mean ± SEM of 15-17 determinations, each from a single cell, recorded in at least three different transfections.

6.13 Molecular modelling of the mechanism through which the R190 residue participates in the stabilization of the closed state of KCNT2 channels

To investigate the molecular mechanisms by which the R190 residue controls gating in KCNT2 channels, we used homology molecular modeling to build a three-dimensional structure of a single KCNT2 subunit in the open or closed configurations. Because high-resolution crystal structures of KCNT2 channels are still unavailable, homology modelling studies were performed using the closed and open configurations of chicken KCNT1 channels resolved by cryo-electron microscopy at 4.5 Å, as template [Hite et al.2015; Hite et al., 2017].

As highlighted in the homology model shown in Figure 28 A, in the closed state of the channel, the R190 residue, forms strong ionized hydrogen bounds with two regions which do not belong to the same subunit. In particular, the R190 residue may interact with the side chain of the E283 residue located in the S_6 and of the Q349 residue located in the RCK1 domain, thus promoting the stabilization of the closed state. In the open state of the channel, the interaction described above could not be detected (Figure 28 B).

These modelling results suggest that the R190 mutation may selectively destabilize the closed state of the channel by impeding these electrostatic interactions, thereby promoting constitutive channel opening.

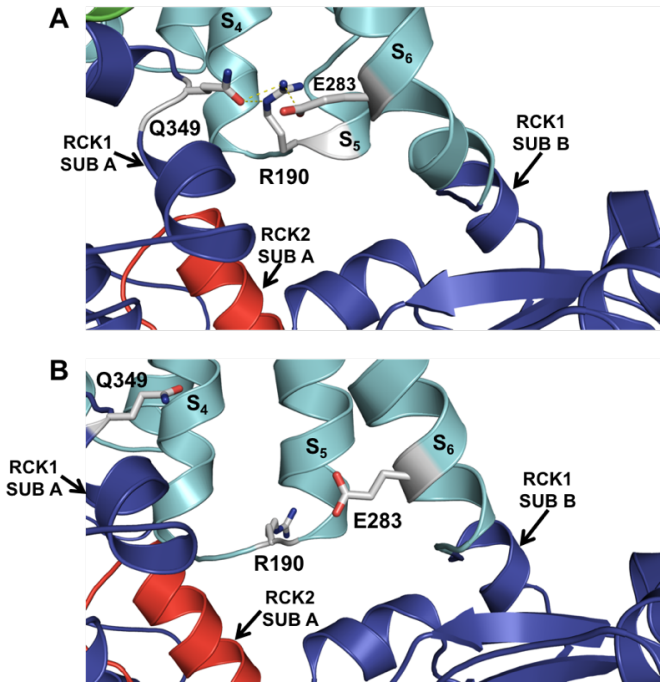

Figure 28 Homology model of the closed state (A) and open state (B) of KCNT2 channels. The R190 residue is involved in the electrostatic interaction occurring between the other residue Q349 and E283 indicated. Transmembrane segments are colored in gray, while RCK1 and RCK2 domains are in blue or red, respectively.

6.14 Pharmacological modulation of wild-type and mutant KCNT2 subunits

The KCNT2 currents are blocked by quinidine in a concentration-dependent manner. Therefore, to evaluate the possibility to counteract the functional alterations induced by the presence of R190H or R190P mutations in KCNT2 channels, we tested 10, 100 and 1000 μM quinidine on both wild-type and mutant KCNT2 subunits. When quinidine was tested on wild-type KCNT2 currents, the IC_{50} of current inhibition at +60 mV was 44 μM, being slightly more sensitive to drug-induced blockade compared to KCNT1 channels (IC_{50} of 82 μM). Notably, when compared to KCNT2, quinidine was more effective and potent in blocking KCNT2 R190H (IC_{50} of 36 μM) or KCNT2 R190P (IC_{50} of 26 μM) channels. In particular, a quinidine concentration of 10 μM was unable to inhibit KCNT2 channels, whereas a highly-significant 20-30% blockade was observed for both KCNT2 R190H- and KCNT2 R190P-mediated currents (Figure 29).

Prompted by these results, physicians added quinidine (starting dose 33 mg/kg) to the standard valproate therapy (300 mg/d) in patient carrying the R190H mutation.

Within the following 4 weeks, clinical status of this patient seems to be improved. In particular, seizure frequency was reduced from daily to 2-3 events per week without apparent side effects.

Given the above mentioned clinical and preclinical data, these results demonstrate that quinidine counteracts the functional alterations induced by the presence of R190H or R190P mutations. Furthermore, these results highlight that K^+ channel blockers, such as quinidine, may represent a targeted therapy for these patients.

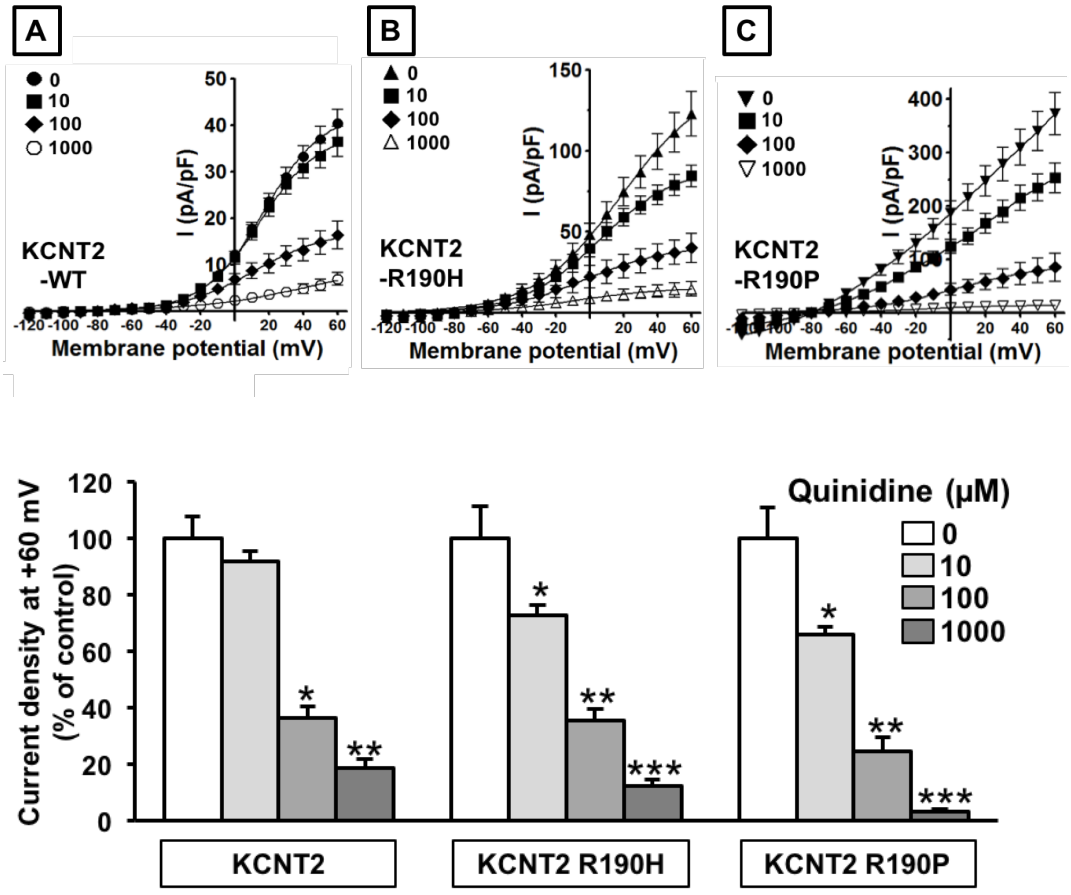

Figure 29 Pharmacological characterization of the currents expressed by wild-type or mutant KCNT2 channels. (A,B,C upper panel) Pooled current density data from HEK-293 cells expressing wild-type or mutant KCNT2 channels, as indicated, in control solution or upon exposure to quinidine at 10,100 or 1000 μM. Lower panel, average of current density measured at +60 mV from HEK cells expressing wild-type or mutant KCNT2 channels, as indicated in the control solution (white bars) or upon exposure to quinidine (10-1000 μM; gray bars); current density was expressed as % of the control current. Single or multiple asterisks indicate values significantly different than that of the previous bar ($p<0.05$).

7. DISCUSSION

Epilepsy is a phenotypically-heterogeneous disease characterized by an enduring predisposition to generate seizures. This pathological condition often leads to neurobiological, cognitive, psychological, and social impairments in the affected patients. [International League Against Epilepsy, 2014]. In a large fraction of epilepsy types, genetic mutations in several genes encoding for ion channels, receptors, or other proteins have been identified.

One of these is represented by the KCNT1 gene, which codes for pore-forming α–subunits of Na^+-dependent K^+ channels (K_{Na}), that play an important role in the regulation of neuronal excitability [Battacharjee et al., 2005]. The KCNT1 channels together with the homologous KCNT2 channels, belong to the SLO2 family of Na^+-activated K^+ channels. KCNT1 channels, as well as KCNT2 channels, consists of six transmembrane segments (S_1-S_6) and an extended C-terminal region that encompasses two predicted RCK (regulators of conductance of K^+) domains. These subunits assemble as tetramers to form functional channels, whose activation is only slightly voltage-dependent [Joiner et al., 1998]. In particular, the voltage-dependence of SLO2 channels activation seems to be regulated by the voltage-dependent binding of Na^+ ions in an intracellular site, at least in part located in the RCK2 domain.

KCNT1 is widely expressed throughout the brain, as well as in the dorsal root ganglia, kidney and heart [Kaczmarek et al., 2013].

To date, *de novo* mutations in the KCNT1 gene have been reported in a wide range of epileptic disorders, particularly in Malignant Migrating Partial Seizure of Infancy (MMPSI). Mutations in the KCNT1 gene have been also shown to be responsible for autosomal-dominant and sporadic cases of nocturnal frontal lobe epilepsy [Heron et al., 2012], as well as in a few cases of Ohtahara syndrome, West syndrome and Brugada syndrome [Juang et al., 2014].

The most common functional effect induced by MMPSI-causing mutations is a gain-of-function effect on KCNT1 channels.

In the present work, I have characterized the biochemical, functional and pharmacological properties of *de novo* heterozygous mutations in the KCNT1 gene (Table 6), found in patients affected by EEs. Almost all the KCNT1 mutations herein investigated are localized in the C-terminal region, particularly in the region encompassing the RCK domains of the channels. By contrast, the G288S mutation falls in the pore S_5 segment of the protein. The results obtained are summarized in the following Table:

		G288S	M516V	E893K	R950Q
KCNT1	Functional phenotype	GOF	GOF	GOF	GOF
	Homomeric channels	↑ current density	↑ current density	↑ current density	↑ current density
	Heteromeric channels	↑ current density	↑ current density	ND	ND
	Voltage dependence of activation	leftward shifted	leftward shifted	leftward shifted	leftward shifted
	Na^+-dependent activation	apparently ↑	apparently ↑	apparently ↑	apparently ↑
	Pharmacological sensitivity to Bepridil	IC_{50} = 0.15±0.05 μM	IC_{50} = 0.3±0.1 μM	ND	ND
	Pharmacological sensitivity to Quinidine	IC_{50} = 46±12 μM	IC_{50} = 67±19 μM	IC_{50} = 9.6±2.5 μM	IC_{50} = 24.0 ± 5.7 μM
	Total protein levels	Not different from WT	↓ compared to WT	Not different from WT	Not different from WT
	Plasma membrane abundance	Not different from WT	↓ compared to WT	ND	ND

Table 6 Summary table of functional results for each mutant KCNT1 subunit studied in this work. GOF=Gain-of-function, ND=Not determined.

Notably, I have also investigated the effects of mutations in the KCNT2 gene, which has never been associated with human disorders. In particular, I studied the effects of an inherited KCNT2 variants, found in a patient affected by ADNFLE (C48AY) and the effects of two *de novo* variants (R190H and R190P) found in two independent patients with EEs. The results obtained are summarized in the following Table:

		C484Y	R190H	R190P
KCNT2	Functional phenotype	No alteration	GOF	GOF
	Homomeric channels	No significantly different versus wild-type	↑ current density	↑ current density
	Heteromeric channels	ND	intermediate current density between homomeric WT and mutant subunits	intermediate current density between homomeric WT and mutant subunits
	Voltage dependence of activation	No difference	leftward shifted	leftward shifted
	Na^+- dependent activation	ND	apparently ↑	apparently ↑
	Pharmacological sensitivity to Quinidine	ND	IC_{50} = 36 μM	IC_{50} = 26 μM
	Total protein level	Not different from WT	Not different from WT	↑ compared to WT

Table 7 Summary table of functional results for each mutant KCNT2 subunit studied in the present work. GOF= Gain-of-function, ND=Not determined.

All the KCNT1 mutations herein investigated induced significant gain-of-function effects, a result consistent with most KCNT1 mutations previously identified in other EE patients. The molecular basis of these effects can be multiple: western-blotting experiments performed in the present work have revealed that the mutation-induced

increase in maximal current does not appear to be related to an increase in total or plasma membrane abundance of KCNT1 subunits carrying specific substitutions, as also reported previously for other epilepsy-causing KCNT1 variants [Kim et al., 2014].

Notably, computational analysis suggests possible changes in the molecular structure and the ion channel property induced by the recurrent G288S mutation. In fact, the G288S substitution introduces a hydrogen bond that alters the pore structure domain, thus altering channel function [Ishii et al., 2013]. A reduction in the unitary conductance and an abolishment of subconductance states were also observed in KCNT1-G288S channels [Kim and Kaczmarek, 2014].

By contrast, no structural insights are available to understand the molecular basis of the gain-of-function effects of the other KCNT1 mutations herein investigated; however, their location within the RCK domains and the alteration in the Na^+-sensitivity observed for the currents elicited by KCNT1 channels carrying each mutation, both suggest a plausible mutation-induced alteration in the RCK structure, therefore leading to an increased channel sensitivity to intracellular Na^+ ions. In addition, the KCNT1 C-terminal region also contains several putative consensus sites for phosphorylation by protein kinase C [Santi et al., 2006]. In particular, one of these sites (T517) is located in the RCK1 domain, immediately past the M516 residue affected by the MMPSI mutation described in the present work. This observation suggests that mutations in the C-terminal region of KCNT1 channels may interfere with the channel modulation by a complex network of regulatory molecules acting upon the RCK domains; however, this hypothesis would merit further investigation. Finally, several cytoplasmic signaling pathways, such as those mediated by FMRP [Brown et al., 2010], which regulates neuronal excitability and protein translation [Zhang et al., 2012]: a possible alteration in the FMRP-induced KCNT1 current modulation prompted by the KCNT1 mutants herein investigated has not been studied, but could not be excluded.

While several pathogenetic variants in the KCNT1 gene have been identified in EEs patients, no evidence is yet available regarding a possible contribution of *de novo* or inherited KCNT2 variants in human disorders. In this study, massive parallel sequencing in two patients with an overlapping spectrum of Developmental and Epileptic Encephalopathy (DEE) identified two pathogenic variants in the KCNT2 gene, namely

R190H and R190P. As observed for mutations in KCNT1, also KCNT2 substitutions at the R190 residue induce gain-of-function effects. Although high-resolution structures of KCNT2 channels are still unavailable, homology modelling using closed and open configurations of chicken KCNT1 channels determined by cryo-electron microscopy suggested that the R190 residue may participate in the stabilization of the closed state by forming polar interactions with the side chains of the residue E283 [Dai et al., 2010] in the S_6 and the Q349 residue located in the RCK1 domain of the channel; furthermore, this interaction could not be detected in the open configuration of KCNT2 channels. These observations support the hypothesis that R190 mutations would selectively destabilize the closed state of the channel by impeding these interactions, thereby promoting the constitutive channel opening. This mechanism is also consistent with the more dramatic functional effects of the positively-charged R residue replacement with a neutral P when compared to the partially-protonated H.

The observation that hyperexcitability diseases, such as MMPSI, are associated to an increased K^+ channels function appears to be counterintuitive, given the inhibitory roles played by K^+ channel in neuronal excitability. However, other epilepsy-causing gain-of-function mutations in K^+ channel genes have been reported previously, including KCNMA1 [Du et al., 2005], KCNJ10 (KIR4.1) [Sicca et al., 2011], KCND2 (Kv4.2) [Lee et al., 2014], KCNH5 (Kv10.2) [Yang et al., 2013] and KCNQ2 (Kv7.2) [Miceli et al., 2015a].

The potential mechanisms involved are heterogeneous, also depending on the specific function played by the different K^+ channels during ontogenesis at distinct cellular and subcellular sites. These include the regulation of neuron-astrocyte cross-talking [Sicca et al., 2011], enhanced Na^+ channels repriming by faster action potentials repolarization [Du et al., 2005], secondary depolarizations caused by over-activation of the hyperpolarization-activated I_h currents [Robinson and Siegelbaum, 2003], and preferential suppression of inhibitory interneurons, leading to an increased excitability of principal neurons [Miceli et al., 2015a]. As an example, mutations in SCN1A gene are responsible for non-functional $Na_V1.1$ channels leading to severe myoclonic epilepsy of infancy (Dravet's syndrome); in these cases, it has been hypothesized that, due to the

preferential expression of Nav1.1 channels in inhibitory interneurons, selective suppression of interneuronal excitability results in an altered balance between inhibitory versus excitatory currents, sufficient to produce seizures [Chopra and Isom; 2014].

In addition, we also report another KCNT2 variant c.1451 G>A (p.C484Y) identified in a patient with a mild phenotypic spectrum disorder associated to Autosomal Dominant Nocturnal Frontal Lobe Epilepsy (ADNFLE). This variant seems to be unable to induce dramatic effects on channel function and could be therefore classified as a KCNT2 polymorphism. Nonetheless, many reasons could be taken into account to explain such results (e.g. the mutation could alter complex KCNT2 regulatory pathways, not herein investigated); therefore, it should be highlighted that this variant has been inherited from a healthy parent and the clinical phenotype is less severe than those reported for the other KCNT2 mutations herein investigated.

Our results on the pathogenetic role of KCNT2 *de novo* variants in severe developmental epilepsies are also in line with a recent study which reports the F240L KCNT2 *de novo* variant, found in a patient with epileptic encephalopathy. The F240L variant seems to be pathogenic since it induces functional alterations, though they are distinct from those herein reported for KCNT2 R190H or KCNT2 R190P mutations: the substitution, falling in the pore of the channel, reduces current inhibition by high [Cl^-] and causes the loss of K^+ ions selectivity [Gururaj et al., 2017]. Further studies will be necessary to deepen our knowledge on the pathogenic role of mutations in this gene identified in epileptic individuals.

Quinidine is predominantly used as an antiarrhythmic agent (class IA) and is approved by the US Food and Drug Administration for that indication, as well as for treatment of *Plasmodium falciparum* malaria. Quinidine is well absorbed in the gastrointestinal tract and is rapidly and widely distributed throughout the body, although its central nervous system penetration is relatively poor. Quinidine is extensively metabolized in the liver by the cytochrome-P450 enzyme system. Thus, quinidine exhibits many drug-drug interactions including inhibition of the metabolism of

many antiepileptic drugs. Due to the effects of quinidine on cardiac conductances, QT prolongation is a common adverse effect. Therefore, quinidine should be used with caution in combination with other medications that may prolong the QT interval, and EKG monitoring should be considered [Kusuhara et al., 1997]. Given that the functional characterization of all the KCNT1 and KCNT2 mutations herein investigated are associated to a significant increase in channel function, we have explored the hypothesis that KCNT channels blockers could be useful to counteract these mutation-induced functional effects [Yang et al., 2006]. Notably, our results revealed that all mutant KCNT1 and KCNT2 channels herein investigated showed a significant increase in current blockade by quinidine and/or bepridil when compared to corresponding wild-type channels. This increased sensitivity of mutant channels could be due to the mutation-induced negative shifts of the activation gating observed in all KCNT1 or KCNT2 mutant channels, leading to an increased availability of mutant channels in the open configuration, that would favor the interaction of bepridil and quinidine with this state of KCNT channels: these results carry novel pharmacogenomics implications for the treatment of epileptic encephalopathies such as MMPSI.

The first report repurposing the use of quinidine in a 3 year-old girl with MMPSI who had 5 to 20 seizures per day, described a marked improvement in seizure control so that she was only experiencing seizures at the time of homeostatic stress, e.g., with intercurrent infection on treatment [Bearden et al., 2014]. Similarly, Milligan and coll. (2014) found a significant effect of quinidine in a patient with MMPSI, but not in a second patient with ADNFLE.

Efficacy of quinidine in MMPSI patients may depend on the underlying genetic mutation, as well as the age of patients and the epileptic phenotype, although a clear genotype-phenotype correlation remains to be clarified [Mikati et al., 2015].

Furthermore, the therapeutic range for quinidine as an anticonvulsant in KCNT1- or KCNT2-realted epilepsies has yet to be established and quinidine use in MMPSI patients in the literature suggests the need for caution in introducing presumed precision therapies for the severe genetic epilepsies.

However, quinidine is a weak antagonist of KCNT channels and has a relatively poor blood-brain barrier penetration and hence may not have achieved sufficient

concentrations in the brain to normalize pathological KCNT conductance. Notably, preliminary results on quinidine treatment of the patient carrying KCNT2-R190H mutation suggest an improvement of the clinical parameters, especially in terms of seizure frequency, although several clinical implications may be considered. In this patient, quinidine serum levels were found to be 0.7 mg/l, a value much lower than the therapeutic plasma range (2–5 mg/l) indicated for its use as an antiarrhythmic [Routledge and Hutchings, 2013]. Given the hypothesized developmental function of KCNT1 channels via interaction with FMRP, it is possible that there was irreversible brain dysfunction prior to initiation of therapy due to aberrant neurodevelopment. Therefore, it is possible that earlier administration of quinidine, such as at the onset of epilepsy or before permanent brain injuries, might produce better results.

In conclusion, the antiarrhythmic compound quinidine may be at least partially effective in the treatment of MMPSI patients carrying gain-of-function KCNT mutations; however, the first randomized trial of oral administration of quinidine (300 mg/d) to 6 patients (adult and teenagers) with ADNFLE due to KCNT1 mutations, showed either adverse events or lacked of efficacy in terms of seizures' frequency [Mullen et al., 2017]. These negative results could be due to many reasons: for example, patients were adults (30-43 years) with ADNFLE and not MMPSI, therefore rendering still more complicated to assess clinical efficacy of quinidine in epileptic patients carrying KCNT mutations.

Further studies are needed to definitively demonstrate the efficacy of quinidine, determine optimum dosing, and verify the effects of earlier initiation of therapy [Bearden et al., 2014].

8. REFERENCES

1. Aoki K, Kosakai K, Yoshino M (2008). Monoaminergic modulation of Na^+-activated K^+ channel in kenyon cells isolated from the mushroom body of the cricket (Gryllus bimaculatus) brain. *Journal of Neurophysiology* 100, 3 1211-1222.
2. Backx L, Ceulemans B, Vermeesch JR, Devriendt K, Van Esch H (2009). Early myoclonic encephalopathy caused by a disruption of the neuregulin-1 receptor ErbB4. *European Journal of Human Genetics* 17(3): 378–382.
3. Barcia G, Fleming MR, Deligniere A, Gazula VR, Brown MR, Langouet M, Chen H, Kronengold J, Abhyankar A, Cilio R, Nitschke P, Kaminska A, Boddaert N, Casanova JL, Desguerre I, Munnich A, Dulac O, Kaczmarek LK, Colleaux L, Nabbout R (2012). De novo gain-of-function KCNT1 channel mutations cause malignant migrating partial seizure of infancy. *Nature Genetics* 44(11):1255-9.
4. Beal JC, Cherian K, Moshe SL (2012). Early-onset epileptic encephalopathies: Ohtahara syndrome and early myoclonic encephalopathy. *Pediatric Neurology* 47(5):317-23.
5. Bearden D, Strong A, Ehnot J, DiGiovine M, Dlugos D, Goldberg EM (2014). Targeted treatment of migrating partial seizures of infancy with quinidine. *Annals of Neurology*. 76, 457–461.
6. Berg AT, Berkovic SF, Brodie MJ, Buchhalter J, Cross JH, van Emde Boas W, Engel J, French J, Glauser TA, Mathern GW, Moshé SL, Nordli D, Plouin P, Scheffer IE (2010). Revised terminology and concepts for organization of seizures and epilepsies: report of the ILAE Commission on Classification and Terminology, 2005-2009. *Epilepsia* 51(4):676-85.
7. Bhattacharjee A and Kaczmarek L (2005). For K^+ channels, Na^+ is the new Ca^{2+}. *Trends in Neuroscience* 28, 422-428.
8. Bhattacharjee A, Joiner WJ, Wu M, Yang Y, Sigworth FJ, Kaczmarek LK (2003). (Slo2.1), a rapidly-gating sodium-activated potassium channel inhibited by ATP. *Journal of Neuroscience* 23(37):11681-91.
9. Bischoff U, Vogel W and Safronov BV (1998). Na^+-activated K^+ channels in small dorsal root ganglion neurones of rat. *Journal of Physiology* 510, 743-754.
10. Biton B, Sethuramanujam S, Picchione KE et al., (2012). The antipsycotic drug loxapine is an opener of the sodium-activated potassium channel slack (Slo2.2). *Journal of Pharmacology and Experimental Therapeutics* 340, 706-715.
11. Brown M, Kronengold J, Gazula V, Spilianakis C, Flavell R, von Hehn C et al., (2008). Amino-termini isoforms of the Slack K^+ channel, regulated by alternative promoters, differentially modulate rhythmic firing and adaptation. *Journal of Physiology* 586,5161-5179.
12. Brown MR, Kronengold J, Gazula VR et al., (2010). Fragile X mental retardation protein controls gating of the sodium-activated potassium channel Slack. *Nature Neuroscience* 13:7, 819-821.
13. Carranza Rojo D, Hamiwka L, McMahon JM, Dibbens LM, Arsov T, Suls A, Stödberg T, Kelley K, Wirrell E, Appleton B, Mackay M, Freeman JL, Yendle SC, Berkovic SF, Bienvenu T, De Jonghe P, Thorburn DR, Mulley JC, Mefford HC, Scheffer IE (2011). De novo SCN1A mutations in migrating partial seizures of infancy. *Neurology* 77(4):380-3.
14. Chen H, Kronengold J, Yan Y, Gazula V, Brown M, Ma L et al., (2009). The N-terminal domain of Slack determinates the formation and trafficking of Slick/Slack heteromeric sodium-activated potassium channels. *Journal of Neuroscience* 29, 5654-5665.

15. Choi M, Scholl UI, Ji W, Liu T, Tikhonova IR, Zumbo P, Nayir A, Bakkaloğlu A, Ozen S, Sanjad S, Nelson-Williams C, Farhi A, Mane S, Lifton RP (2009). Genetic diagnosis by whole exome capture and massively parallel DNA sequencing. *Proceedings of the National Academy of Science* 106(45):19096-101.
16. Chopra R, Isom LL (2014). Untangling the dravet syndrome seizure network: the changing face of a rare genetic epilepsy. Epilepsy Currents 14(2):86-9.
17. Claes L, Del-Favero J, Ceulemans B, Lagae L, Van Broeckhoven C, De Jonghe P (2001). De novo mutations in the sodium-channel gene SCN1A cause severe myoclonic epilepsy of infancy. *American Journal of Human Genetics* 68(6):1327-32.
18. Coppola G, Plouin P, Chiron C, Robain O, Dulac O (1995). Migrating partial seizure in infancy: a malignant disorder with developmental arrest. *Epilepsia* 36(10):1017-24.
19. Dai L, Garg V, Sanguinetti M (2010). Activation of Slo2.1 channels by niflumic acid. *The Journal of General Physiology* 135(3): 275–295.
20. Deciphering Developmental Disorders S. Prelevance and architecture of de novo mutations in developmental disorders (2017). *Nature* 542(7642):433-8.
21. Dryer SE (1994). Na^+-activated K^+ channels: a new family of large conductance ion channels. *Trends in Neuroscience* 17:155-160.
22. Du W, Bautista JF, Yang H, Diez-Sampedro A, You SA, Wang L, Kotagal P, Luders HO, Shi J, Cui J, Richerson GB, Wang QK (2005). Calcium-sensitive potassium channelopathy in human epilepsy and paroxysmal movement disorder. *Nature Genetics* 37, 733–738.
23. Dulac O, (2005). Malignant migrating partial seizure in infancy. In Roger J, Bureau M, Dravet Ch, Genton P, Tassinari CA, Wolf O (Eds) Epileptic syndromes in infancy, childhood and adolescence, 4th edn. John Libbey Eurotext Ltd, Montrouge, France, pp73-76.
24. Evely KM, Pryce KD, Bhattacharjee A (2017). The Phe932Ile mutation in KCNT1 channels associated with severe epilepsy, delayed myelination and leukoencephalopathy produces a loss-of-function channel phenotype. *Neuroscience* 20; 351:65-70.
25. Fisher RS, van Emde Boas W, Blume W, Elger C, Genton P, Lee P, Engel J Jr (2005). Epileptic seizures and epilepsy: definitions proposed by the International League Against Epilepsy (ILAE) and the International Bureau for Epilepsy (IBE). *Epilepsia.* 46(4):470-2.
26. Gonzalez C, Baez-Nieto, Valencia I, Oyarzùn I, Rojas P, Naranjo D, Latorre R (2012). K^+ channels: Function-Structural Overview. *Comprehensive Physiology* 2(3):2087-149.
27. Gorman AL and Thomas MV (1980). Potassium conductance and internal calcium accumulation in a molluscan neurone. *Journal of Physiology* 308, 287-313.
28. Gururaj S, Palmer EE, Sheehan GD, Kandula T, Macintosh R, Ying K, Morris P, Tao J, Dias KR, Zhu Y, Dinger ME, Cowley MJ, Kirk EP, Roscioli T, Sachdev R, Duffey ME, Bye A, Bhattacharjee A (2017). A de novo mutation in the Sodium-Activeted Potassium Channel KCNT2 aters ion selectivity and cause Epileptic Encephalopathy. *Cell Reports*. 21(4):926-933
29. Gustaffsson B and Wingstrom H (1983). Hyperpolarization following long-lasting tetanic activation of hippocampal pyramidal cells. *Brain Research* 275, 159-169.
30. Hage TA, Salkoff L (2012). Sodium-Activated Potassium Channels are Functionally Coupled to Persistent Sodium Currents. *The Journal of Neuroscience* 32(8):2714-2721.
31. Hartung K (1985). Potentiation of a transient outward current by Na+ influx in crayfish neurones. *Pflugers Archiv-European Journal of Physiology* 404(1):41-4.
32. Heilbig I, von Deimling M, Marsh ED (2017) Epileptic Encephalopathies as neurodegenerative disorders. *Advances in Neurobiology* 15:295-315.

33. Helbig KL, Farwell Hagman KD, Shinde DN, Mroske C, Powis Z, Li S, Tang S, Helbig I (2016). Diagnostic exome sequencing provides a molecular diagnosis for a significant proportion of patients with epilepsy. *Genetics in Medicine* 18(9):898-90.

34. Heron SE, Smith KR, Bahlo M et al., (2012). Missense mutations in the sodium-activated potassium channel gene KCNT1 cause severe autosomal dominant nocturnal frontal lobe epilepsy. *Nature Genetics* 44(11):1188-90.

35. Hite RK, MacKinnon R. (2017). Structural Titration of Slo2.2, a Na+-Dependent K+ Channel. *Cell* 168(3):390-399

36. Hite RK, Yuan P, Li Z, Hsuing Y, Walz T, MacKinnon R (2015). Cryo-electron microscopy structure of the Slo2.2 Na(+)-activated K(+) channel. *Nature* 527(7577):198-203.

37. Hmaimess G, Kadhim H, Nassogne MC, Bonnier C, van Rijckevorsel K (2006). Levetiracetam in a neonate with malignant migrating partial seizures. *Pediatric Neurology* 34(1):55-9.

38. Ishii A, Shioda M, Okumura A, Kidokoro H, Sakauchi M, Shimada S, Shimizu T, Osawa M, Hirose S, Yamamoto T (2013). A recurrent KCNT1 mutation in two sporadic cases with malignant migrating partial seizure of infancy. *Gene* 531, 467-471.

39. Jacobson MP, Pincus DL, Rapp CS et al., (2004). A hierarchical approach to all-atom protein loop prediction. *Proteins* 55(2):351-67.

40. Joiner WJ, Tang MD, Wang LY, Dworetzky SI, Boissard CG, Gan L, Gribkoff VK, Kaczmarek LK (1998). Formation of intermediate –conductance calcium-activated potassium channels by interaction of Slack and Slo subunits. *Nature Neuroscience* 1, 462-469.

41. Juang JM, Lu TP, Lai LC, Ho CC, Liu YB, Tsai CT, Lin LY, Yu CC, Chen WJ, Chaing FT, Yeh SF, Lai LP, Chuang EY, Lin JL (2014). Disease-targeted sequencing of ion channel genes identifies de novo mutations in patients with non-familial Brugada syndrome. *Scientific Report* 4, 6733.

42. Kaczmarek LK (2013). Slack, Slick and Sodium-Activated Potassium Channels. *Journal of Neuroscience* 2013:354262.

43. Kameyama M et al., (1984). Intracellular Na^+ activates K^+ channels in mammalian cardiac cells. *Nature* 309, 354-356.

44. Kim G and Kaczmarek L (2014). Emerging role of the KCNT1 Slack channel in intellectual disability. Frontiers in Cellular Neuroscience 28, 8:209.

45. Kim GE, Kronengold J, Barcia G, Imran HQ, Martin HC, Blair E, Taylor JC, Dulac O, Colleaux L, Nabbout, Kaczmarek KL (2014). Human Slack potassium channel mutations increase positive cooperativity between individual channels. *Cell reports*. 2014;9(5):1661-1672.

46. Kurahashi H and Hirose S In Adam MP, Ardinger HH, Pagon RA, Wallace SE, Bean LJH, Mefford HC, Stephens K, Amemiya A, Ledbetter N, editors (2015). Autosomal Dominant Nocturnal Frontal Lobe Epilepsy. *GeneReviews®*

47. Kusuhara H, Suzuki H, Terasaki T, et al. (1997). P-glycoprotein mediates the efflux of quinidine across the blood-brain barrier. *The Journal of pharmacology and experimental therapeutics* 283:574–580.

48. Lee H, Lin MC, Kornblum HI, Papazian DM, Nelson SF, (2014). Exome sequencing identifies de novo gain of function missense mutation in KCND2 in identical twins with autism and seizures that slows potassium channel inactivation. Human Molecular Genetics 23, 3481–3489.

49. Li Y, Sato T, Arita M (1999) Bepridil blunts the shortening of action potential duration caused by metabolic inhibition via blockade of ATP-sensitive K^+ channels and Na^+-activated K^+ channels. *Journal of Pharmacology and Experimental Therapeutics* 291:2, 562-568.

50. Lim CX, Ricos MG, Dibbens LM, Heron SE (2016). KCNT1 mutations in seizure disorders: the phenotypic spectrum and functional effects. *Journal of Medical Genetics* 53(4):217-25.

51. Martin HC, Kim GE, Pagnamenta AT, Murakami Y, Carvill GL, Meyer E, Copley RR, Rimmer A, Barcia G, Fleming MR, Kronengold J, Brown MR, Hudspith KA, et al., (2014). Clinical whole-exome sequencing in severe early-onset epileptic epilepsy reveal new genes and improves molecular diagnosis. *Human Molecular Genetics* 23, 3200-3211.

52. Martinez-Espinosa PL, Wu J, Yang C, Gonzalez-Perez V, Zhou H, Liang H, Xia XM, Lingle CJ (2015). Knockout of Slo2.2 enhances itch, abolishes KNa current, and increases action potential firing frequency in DRG neurons. *Elife* 11,4.

53. Mc Tague A, Appleton R, Avula S, Cross JH, King M D, Jacques T S, Bhate S, Cronin A, Curran A, Desurkar A, Farrell M A, Hughes E, Jefferson R, Lascelles K, Livingston J, Meyer E, McLellan A, Poduri A, Scheffer I E, Spinty S, Kurian M A, and Kneen R (2013) Migrating partial seizures of infancy: expansion of the electroclinical, radiological and pathological disease spectrum. *Brain* 136(5): 1578–1591.

54. Mefford HC. Clinical Genetic Testing in Epilepsy. *Epilepsy Currents*. 2015;15(4):197-201.

55. Miceli F, Soldovieri MV, Ambrosino P, De Maria M, Migliore M, Migliore R Taglialatela M (2015a) Early-onset epileptic encephalopathy caused by gain-of-function mutations in the voltage sensor of Kv7.2 and Kv7.3 potassium channel subunits. *The Journal of Neuroscience* 35: 3782–3793.

56. Mikati MA, Jiang YH, Carboni M, Shashi V, Petrovski S, Spillmann R, Milligan CJ, Li M, Grefe A, McConkie A, Berkovic S, Scheffer I, Mullen S, Bonner M, Petrou S, Goldstein D (2015). Quinidine in the treatment of KCNT1-positive epilepsies. *Annals of Neurology* 78(6):995-9.

57. Milh M, Falace A, Villeneuve N, Vanni N, Cacciagli P, Assereto S, Nabbout R,Benfenati F, Zara F, Chabrol B, Villard L, Fassio A (2013). Novel compound heterozygous mutations in TBC1D24 cause familial malignant migrating partial seizures of infancy. *Human Mutation* 34(6):869-72.

58. Milligan CJ, Li M, Gazina EV, Heron SE, Nair U, Trager C, Reid CA, Vankat A, Younkin DP, Dlugos DJ, Petrovski S, Goldstein DB, Dibbens LM, Scheffer IE, Berkovic SF, Petrou S (2014). KCNT1 gain of function in 2 epilepsy phenotypes is reversed by quinidine. *Annals of Neurology* 75, 581-590.

59. Mitani A and Shattock MJ (1992). Role of Na^+-activated K^+ channels, Na^+ -K^+ -Cl^- cotransport, and Na^+-K^+ pump in $[K]_e$ changes during ischemiain rat heart. *American Journal of Physiology*, 263, H333-340.

60. Molinari F, Raas-Rothschild A, Rio M, Fiermonte G, Encha-Razavi F, Palmieri L, Palmieri F, Ben-Neriah Z, Kadhom N, Vekemans M, Attie-Bitach T, Munnich A, Rustin P, Colleaux L (2005). Impaired mitochondrial glutamate transport in autosomal recessive neonatal myoclonic epilepsy. *The American Journal of Human Genetics*. 76(2):334-9.

61. Møller RS, Heron SE, Larsen LH, Lim CX, Ricos MG, Bayly MA, van Kempen MJ, Klinkenberg S, Andrews I, Kelley K, Ronen GM, Callen D, McMahon JM, Yendle SC, Carvill GL, Mefford HC, Nabbout R, Poduri A, Striano P, Baglietto MG, Zara F, Smith NJ, Pridmore C, Gardella E, Nikanorova M, Dahl HA, Gellert P, Scheffer IE, Gunning B, Kragh-Olsen B, Dibbens LM (2015). Mutations in KCNT1 cause a spectrum of focal epilepsy. *Epilepsia* 56(9).

62. Mori K, Saito T, Masuda Y, Nakaya H (1998). Effects of class III antiarrhythmic drug on the Na^+-activated K^+ channels in guinea-pig ventricular cells. *Naunyn-Schmiedeberg's Archives of Pharmacology* 358,6 641-648.

63. Mullen SA, Carney PW, Roten A, Ching M, Lightfoot PA, Churilov L, Nair U, Li M, Berkovic SF, Petrou S, Scheffer IE (2017). Precision therapy for epilepsy due to

KCNT1 mutations: a randomized trial of oral quinidine. *Neurology* [Epub ahead of print].

64. Nakamura K, Kato M, Osaka H, Yamashita S, Nakagawa E, Haginoya K, et al., (2013). Clinical spectrum of SCN2A mutations expanding to Ohtahara syndrome. *Neurology* 81, 992-998.

65. Nieh SE and Sherr EH (2014). Epileptic Encephalopathies: New Genes and New Pathways. *Neurotherapeutics* 11(4): 796–806.

66. Ohtahara S, Ishida T, Oka E, Yamatogy Y, Inoue H (1976). On the specific age-dependent epileptic syndromes: The early-infantile epileptic encephalopathy with suppression-burst. *No To Hattatsu***,** 8, pp. 270-280

67. Rizzi S, Knaus HG, Schwarzer C (2016). Differential distribution of the sodium-activated potassium channels Slick and Slack in mouse brain. *Journal of Comparative Neurology* 524(10): 2093–2116.

68. Rizzo F, Ambrosino P, Guacci A, Chetta M, Marchese G, Rocco T, Soldovieri MV, Manocchio L, Mosca I, Casara G, Vecchi M, Taglialatela M, Coppola G, Weisz A (2016). Characterization of two de novo KCNT1 mutations in children with malignant migrating partial seizures in infancy. *Molecular and Cellular Neuroscience* 72:54-63.

69. Robinson RB, Siegelbaum SA, (2003). Hyperpolarization-activated cation currents: from molecules to physiological function. *Annual Review of Physiology* 65, 453–480.

70. Routledge and Hutchings The Immunoassay Handbook (4th) Theory and Applications of Ligand Binding, ELISA and Related Techniques 2013.

71. Saitsu H, Kato M, Koide A, Goto T, Fujita T, Nishiyama K et al., (2012a). Whole exome sequencing identifies KCNQ2 mutatations in Ohtahara syndrome. *Annals of Neurology* 72, 298-300.

72. Salkoff L, Butler A, Ferreira G, Santi C and Wei A (2006). High-conductance potassium channels of the SLO family. *Nature reviews Neuroscience* 7(12):921-931.

73. Santi C, Ferreira G, Yang B, Gazula V, Butler A, Wei A et al., (2006). Opposite regulation of Slick and Slack K^+ channels by neuromodulators. *Journal of Neuroscience* 26, 5059-5068.

74. Scheffer IE, Berkovic S, Capovilla G et al., (2017). ILAE classification of the epilepsies: Position paper of the ILAE Commission for Classification and Terminology. *Epilepsia* 58(4):512-521.

75. Schwindt PC, Spain WJ, Foehring RC, Chubb MC, Crill WE (1988a). Slow conductances in neurons from cat sensorimotor cortex *in vitro* and their role in slow excitability changes. *Journal of Neurophysiology* 59, 450-467.

76. Schwindt PC, Spain WJ, Foehring RC, Stafstrom CE, Chubb MC, Crill WE (1988b). Multiple potassium conductances and their functions in neurons from cat sensorimotor cortex *in vitro*. *Journal of Neurophysiology* 59, 424-449.

77. Sicca F, Imbrici P, D'Adamo MC, Moro F, Bonatti F, Brovedani P, Grottesi A, Guerrini R, Masi G, Santorelli FM, Pessia M, (2011). Autism with seizures and intellectual disability: possible causative role of gain-of-function of the inwardly-rectifying K+ channel Kir4.1. *Neurobiology Disease* 43, 239–247.

78. Singh NA, Charlier C, Stauffer D, DuPont BR, Leach RJ, Melis R, Ronen GM, Bjerre I, Quattlebaum T, Murphy JV, McHarg ML, Gagnon D, Rosales TO, Peiffer A, Anderson VE, Leppert M (1998). A novel potassium channel gene, KCNQ2, is mutated in an inherited epilepsy of newborns. *Nature Genetics* 18(1):25-9.

79. Steinlein OK, Mulley JC, Propping P, Wallace RH, Phillips HA, Sutherland GR, Scheffer IE, Berkovic SF (1995). A missense mutation in the neuronal nicotinic acetylcholine receptor alpha 4 subunit is associated with autosomal dominant nocturnal frontal lobe epilepsy. *Nature Genetics* 11(2):201-3.

80. Sugawara T, Miyazaki E, Fukushima K, Shimomura J, Fujiwara T, Hamano S, Inoue Y and Yamakawa K (2002). Frequent mutations of SCN1A in severe myoclonic epilepsy in infancy. *Neurology* 58:1122-1124.
81. Tamsett TJ, Picchione KE and Bhattacharjee A (2009). NAD^+ activates K_{Na} channels in dorsal root ganglion neurons. *Journal of Neuroscience* 29, 5127-5134.
82. Tejada MD, Jensen LJ, Klaerke DA (2012). PIP(2) modulation of Slick and Slack K^+ channels. *Biochemical and Biophysical Research Communications* 424, 208-213.
83. Tomita S, Nicoll RA, Bredt DS (2001). PDZ protein interactions regulating glutamate receptors function and plasticity. *Journal of Cell Biology* 153(5):F19-24.
84. Villa C and Combi R (2016). Potassium channels and Human Epileptic Phenotypes: an updated overview. *Frontiers in Cellular Neuroscience* 10: 81.
85. Wallen P, Robertson B, Cangiano L, Low P, Bhattacharjee A, Kaczmarek LK et al., (2007). Sodium-dependent potassium channels of a Slack-like subtype contribute to the slow afterhyperpolarization in lamprey spinal neurons. *Journal of Physiology* 585, 75-90.
86. Watanabe T, Sadamoto H, Aonuma H. (2013). Molecular basis of the dopaminergic system in the cricket Gryllus bimaculatus. *Invertebrate Neuroscience*. 13(2):107-23.
87. Yang B, Desai R, Kaczmarek LK (2007). Slack and Slick K(Na) channels regulate the accuracy of timing of auditory neurons. *Journal of Neuroscience* 27(10):2617-27.
88. Yang B, Gribkoff VK, Pan J, Damagnez SI, Boissard CG, Bhattacharjee A, Yan Y, Sigworth FJ, Kaczmarek LK (2006). Pharmacological activation and inhibition of Slack (2.2) channels. *Neuropharmacology* 51, 896-906.
89. Yang Y, Vasylyev DV, Dib-Hajj F, Veeramah KR, Hammer MF, Dib-Hajj SD, Waxman SG, (2013). Multistate structural modeling and voltage-clamp analysis of epilepsy/autism mutation Kv10.2-R327H demonstrate the role of this residue in stabilizing the channel closed state. *Journal of Neuroscience* 33, 16586–16593.
90. Yuan A, Dourado M, Butler A, Walton N, Wei A and Salkoff L (2000). SLO-2, a K^+ channel with an unusual Cl^- dependence. *Nature Neuroscience* 3, 771-779.
91. Yuan A, Santi C, Wei A et al., (2003). The sodium-activated potassium channel is encoded by a member of the Slo gene family. *Neuron* 37(5):765-773.
92. Zhang L, Sukhareva M, Barker JL et al., (2005). Direct binding of estradiol enhances Slack (sequence like a calcium-activated potassium channel) channels activity. *Neuroscience* 131, 275-282.
93. Zhang Z, Rosenhouse-Dantsker A, Tang QY, Noskov S, Logothetis DE (2010). The RCK2 domain uses a coordination site present in Kir channels to confer sodium sensitivity to Slo2.2 channels. *Journal of Neuroscience* 30(22):7554-62.
94. Zhang, Y., Brown, M.R., Hyland, C., Chen, Y., Kronengold, J., Fleming, M.R., Kohn, A.B., Moroz, L.L., Kaczmarek, L.K. (2012). Regulation of neuronal excitability by interaction of fragile X mental retardation protein with slack potassium channels. *Journal of Neuroscience* 32, 15318–15327.

9. ACKNOWLEDGEMENTS

*I would like to express my sincere thankfulness to my supervisor **Prof. Maurizio Taglialatela** for all given opportunities during my PhD.*

*Thanks to **Dr. Maria Virginia Soldovieri** for her* guidance *and precious support during the entire period of my PhD course.*

*Thanks to **Dr. Paolo Ambrosino** and Dr. **Ilaria Mosca** for their hard work done for electrophysiological experiments.*

*Thanks to all my collegues **Michela De Maria, Ilaria Mosca**, **Alessandro Medoro**, **Donatella Mignogna** for their friendship and for sharing every moments in lab.*

*Thanks to **Fabrizio** and **my family** for their important support during these years, for their presence…for their existence.*